Norwegian
University of
Life Sciences

Master's Thesis 2023 30 ECTS
Faculty of Science and Technology

Exploring Rate of Change of Frequency (RoCoF) Events in the Nordic Synchronous Area from 2015 to 2023

Kristian Aarsvoll Bø
Environmental Physics and Renewable Energy

Abstract

As the world moves towards a sustainable and emission-free future, the power grid emerges as a key participant in providing electrical energy. With the demand for electrical energy rising, the power grid is challenged with larger loads. These higher loads, combined with more penetration of the lower inertia power sources, wind and solar, challenge the stability of the grid. A part of the power-grid stability is its frequency, which should be kept stable at all times. This thesis explores whether there has been an increase in the Rate of Change of Frequency (RoCoF) events in the Nordic Synchronous Area (NSA) from 2015 to 2023. Where the NSA consists of the power grids of Norway, Sweden, Finland, and a part of Denmark.

The aim is to identify whether there has been an increase in the frequency or severity of RoCoF events, which are critical indicators of grid stability. To perform this, the analysis utilises a comprehensive dataset of power-grid frequency measurements provided by Fingrid, the Finnish transmission system operator. To ensure accuracy and reliability in the findings, the data undergoes extensive processing, including cleaning and smoothing. Smoothing techniques are applied to filter out noise and prepare the data for precise RoCoF calculations. This preparation is crucial for accurately detecting and analysing RoCoF events, setting the stage for a robust analysis.

From the RoCoF analysis, results show that the total number of events is not increasing. However, it is revealed that there is a remarkable increase in the severity of RoCoF events. Specifically, the number of RoCoF events in the range 100–160 $\mathrm{mHz\,s^{-1}}$ averaged about four events annually in the period 2015–2021. This number has increased drastically for the years 2022 and 2023, which had 17 and 12 events. This increasing trend is also found in the ranges above 100–160 $\mathrm{mHz\,s^{-1}}$. Where the analysis finds an annual increase in RoCoF events from 2020 to 2023.

In summary, this thesis demonstrates that RoCoF events within the NSA have shifted and become more severe from 2015 to 2023. The findings are crucial for Transmission System Operators in the NSA, highlighting the need for enhanced monitoring techniques and the development of advanced grid management.

Sammendrag

Etter hvert som verden beveger seg mot en bærekraftig og utslippsfri fremtid, blir strømnettet en sentral aktør i forsyningen av elektrisk energi. Når etterspørselen etter elektrisk energi øker, utfordres kraftnettet med større belastninger. Disse høyere belastningene, kombinert med økt innslag av kraftkilder med lavere treghet, som vind- og solenergi, utfordrer stabiliteten i kraftnettet. En del av stabiliteten til kraftnettet er frekvensen, som bør holdes stabil til enhver tid. Denne avhandlingen undersøker om det har vært en økning i raske frekvensendringer (Rate of Change of Frequency, RoCoF) i det nordiske synkronområdet fra 2015 til 2023. Hvor det nordiske synkronområdet består av kraftnettene i Norge, Sverige, Finland og en del av Danmark.

Målet med avhandlingen er å identifisere om det har vært en økning i hyppigheten eller alvorlighetsgraden av RoCoF-hendelser, som er kritiske indikatorer for nettstabilitet. Analysen benytter et omfattende datasett med frekvensmålinger fra Fingrid, den finske systemoperatøren. For å sikre nøyaktighet og pålitelighet i resultatene gjennomgår dataene omfattende behandling, inkludert rensing og jevning. Jevningsteknikker brukes for å filtrere bort støy og forberede dataene for nøyaktige RoCoF-beregninger. Denne forberedelsen er avgjørende for å kunne oppdage og analysere RoCoF-hendelser på en nøyaktig måte, noe som legger grunnlaget for en robust analyse.

Resultatene fra RoCoF-analysen viser at det totale antallet hendelser ikke øker. Det viser seg imidlertid at det er en bemerkelsesverdig økning i alvorlighetsgraden av RoCoF-hendelser. Antallet RoCoF-hendelser i området 100–160 $\mathrm{mHz\,s^{-1}}$ var i gjennomsnitt omtrent fire hendelser årlig i perioden 2015–2021. Dette antallet har økt drastisk i årene 2022 og 2023, som hadde henholdsvis 17 og 12 hendelser. Denne økende trenden finnes også i områdene over 100–160 $\mathrm{mHz\,s^{-1}}$. Her finner analysen at RoCoF-hendelser øker årlig fra 2020 til 2023.

Oppsummert viser denne avhandlingen at RoCoF-hendelser i det nordiske synkronområdet har endret seg og blitt mer alvorlige fra 2015 til 2023. Funnene er avgjørende for systemansvarlige operatører i det nordiske synkronområdet, og understreker behovet for overvåkingsteknikker og utvikling av avansert nettstyring.

Acknowledgements

This thesis marks the end of my five years at NMBU. It has been a great experience with countless hours spent studying, attending lectures and sitting behind a screen (covid).

The work conducted in this thesis would not have been completed without guidance from my advisor, Leonardo Rydin Gorjão. He has gone above and beyond to provide excellent feedback and suggestions for both my analysis and writing. Thank you, Leo, for putting in the hours to provide excellent feedback for me and the other students you advised this spring.

I would like to thank my family, who have supported and encouraged me throughout the writing process. Encouraging words, great meals, and hugs during my trips home have been much needed. I also want to thank my flatmates for supporting, cheering, and making our flat a comfortable and relaxing environment.

Lastly, I would like to thank Steinar, Tore, and Bjarte, who have made the writing process more enjoyable through their relaxed and humorous conversations.

Patience and
Diligence, like
Faith, remove
Mountains

William Penn (1644–1718)

Kristian Aarsvoll Bø

Oslo, May 2024

Contents

List of Figures

1 Introduction

The United Nations Intergovernmental Panel on Climate Change (IPCC) have, in their Synthesis Report [1], concluded that human activity is the cause of global warming. Global surface temperatures (GST) have, in the period 2011–2022, risen by 1.1 °C, compared to the average from 1850–1900. If the current trend of increasing global warming is not acted upon, the consequences will be severe. The risk of disruption of livelihoods, food security, water supply, human security, and economic growth is projected to increase if the GST reaches 1.5 °C [1]. With consequences increasing in both severity and global reach if the GST rises by 2, 3 or 4 °C above the average.

It is, therefore, crucial to lower the emissions of greenhouse gasses. At the status quo, the use of fossil fuels enables economic growth, transportation, heating, and the generation of electrical power, among others. Currently, energy use from fossil fuels makes up close to 80 percent of the world's total energy usage, according to the International Energy Agency [2]. The challenge to reduce greenhouse gas emissions while transitioning to renewable energy sources (RES) may be the most important and difficult challenge humanity has faced. To overcome this challenge, the use of fossil fuels needs to be reduced, and the world needs sustainable and pollution-free energy. The most preferable candidate for this is electric energy, as it is a high-quality energy carrier. That is, it can be used to produce lower-quality energy, such as heat. One disadvantage with electrical energy is that it is not as easily stored as fossil fuels are. Therefore, electric energy consumption in a power grid must always be matched by production. If the future energy sector is to be almost exclusively based on electricity, power grids also need to be prepared for this change. The power grids in use worldwide vary in quality and reliability. Some areas are without electricity for hours or days at a time, severely hampering economic and technological progress reliant on electricity. It is important to improve and develop power grids in these areas. Additionally, another crucial task is to ensure that current well-functioning power grids are capable of handling future loads and the introduction of more RES. The stability of power grids can be challenged by large shares of volatile RES, such as wind and solar generation. This reduces stabilizing inertia in a power grid, which has traditionally been provided by synchronous generators. This issue has already been encountered by countries like Ireland [3], and is likely also to affect other regions that are converting to, or incorporating, more RES in their grids.

The countries which make up the Nordic Synchronous Area (NSA), Finland, Sweden, Norway, and part of Denmark, have all committed to the European Union's goal of net zero greenhouse gas emissions [4]. Their respective governments have all stated that they aim to reach this goal by 2050 or earlier [5, 6, 7, 8]. Today, the countries in the NSA predominantly produce electric power from hydro- and nuclear power plants. With the climate goals in mind, there has been a rise in the implementation and use of power generated by low-inertia RES around the world, as well as in the NSA. This increase in low-inertia RES produces power without the emission of greenhouse gasses, but RES also challenges the stability of the power grid within the NSA. Traditionally, stability in the power grid has been ensured by synchronous generators, which provide inertia that offers a dampening effect to the power-grid frequency when power generation and consumption vary. With less inertia, the power grid is prone to becoming less

stable and more susceptible to power-grid frequency deviations. These instabilities in the power-grid frequency are commonly called rate of change of frequency (RoCoF) events. They can, in the worst cases, cause disruptions or even blackouts in the grid. The stability of the grid is therefore monitored by measuring the frequency, and load shedding and power generation are used to keep the frequency at 50 Hz. While the introduction of more RES might be connected to increased RoCoF events, this thesis will only perform exploratory work on the power-grid frequency in the NSA. The goal of this thesis is to explore whether the frequency stability of the NSA has changed from 2015 to 2023. This will be done by analysing power-grid frequency data from the Finnish transmission system operator Fingrid [9].

1.1 Research question

Have the number or severity of RoCoF events increased in the NSA from 2015 to 2023?

2 Theory

2.1 The Nordic Synchronous Area

The NSA is a synchronous area containing the national power grid systems of Finland, Sweden, Norway, and part of Denmark. All of these subsystems have their own operator, which are Fingrid (Finland), Svenska Kraftnät (Sweden), Statnett (Norway), and Energinet (Denmark). Together, they are responsible for balancing power production with consumption and ensuring grid function and stability. Electrical power in the NSA has historically mainly been supplied by hydro and nuclear power plants. This is now shifting, as there is an increasing amount of power being generated by wind and solar. Looking closer at energy production, the countries in the NSA combined produced 444 TWh of energy in 2023. With wind and solar installations increasing, this number is expected to increase to 546 TWh by 2030 [10]. As mentioned in the introduction, inertia plays a role in providing stability for power systems, and the NSA is no exception. The installed maximum capacity of inertia-based generation in 2017 was found to be around 95 GW, with generation capacity not providing inertia only making up around 15 GW [11].

After the liberalisation of the power markets within each of the Nordic countries, the power market NordPool was established in 1996. This marketplace for power enabled the trade of power between countries [12]. Since then, the NSA has been further connected to synchronous grids in Europe. The latest addition is a 720 km long, 1400 MW sub-sea high-voltage direct current (HVDC) cable cable connecting Norway to Great Britain [13].

The transmission system operators (TSOs) in the NSA were also early adopters of a common body to enable greater cooperation between TSOs. Making them some of the first countries in the world to trade power across borders. The established body, called Nordel, was founded in 1963. It was dismissed in 2009, and tasks were handed over to the European Network of Transmission System Operators for Electricity (ENTSO-E) [14]. Today the synchronous areas across Europe are all trading power between them. An overview of these different synchronous areas is displayed in Fig. 1. Note that the figure is not up to date, as Ukraine and Moldova have been connected to Continental Europe since 2022 [15].

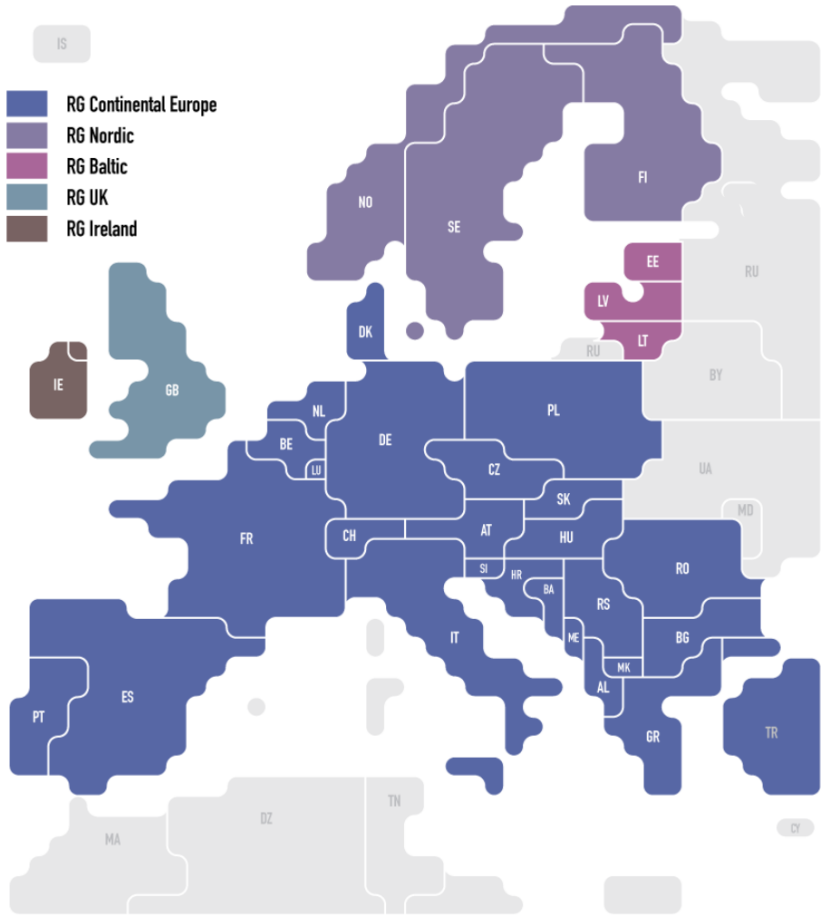

Figure 1: This map shows the different synchronous areas in Europe. The grids in order are RG Contintinetal Europe (blue), RG Nordic (purple), RG UK (green), RG Ireland (brown), and RG Baltic (violet). The figure is taken from [16].

2.2 The power grid

A power grid is an intermediary between the electrical power producer and the consumer. It enables power consumers to be scattered away from the producer by transferring electrical power in high-voltage cables from the producers to the consumers. The physical states in which power grids operate have varied greatly. Earlier power systems operated at various frequencies, including 25, 50, 60, and 133 Hz. Today's standard in the United States is 60 Hz, while 50 Hz is the standard in Europe. Voltage levels are also crucial in power grids and have, since power grids emerged, varied. Today, electrical power is distributed across large distances, far from where it is generated. This is achieved by using high voltages and a lower current. This allows for lesser power loss in transfer. Equations (1), (2), and (3) give context to this claim [17].

The average power P_{ave}, given in watts, follows

$$P_{ave} = I_{rms} V_{rms}, \tag{1}$$

where I_{rms} is the root mean squared current in amperes and V_{rms} is the root mean squared

voltage. From equation (1), one can show that the same amount of power, P_{ave}, can be transferred with differing values of I_{rms} and V_{rms}. This is as long as the product of I and V remain consistent [18].

The V_{rms}, which is the root mean squared voltage, follows

$$V_{rms} = I_{rms} R_{tot}, \tag{2}$$

where I_{rms} is the root mean squared current in ampere and R_{tot} is the total resistance in ohms [18].

By using equation (2) and substituting it into equation (1), one can obtain equation (3). The average power transferred, P_{ave}, now follows

$$P_{ave} = I_{rms}^2 R_{tot}. \tag{3}$$

As seen in equation (3), an increase in current causes the losses to increase quadratically. Because of this relation, the power grid is constructed with different voltage levels, where higher voltages are used to transfer power over greater distances to mitigate losses [18].

The power grid is divided into sections, with transmission, regional, and distribution being the different levels of the grid. Grids in the same synchronous are typically operated with alternating current (AC), as it does not require converter stations like HVDC does. The transmission grids operate at the highest voltages in a grid. As an example, the transmission grid in Norway operates in the voltage ranges of 300 kV and 420 kV. Transmission grids are adept at mitigating losses and transferring power over large distances. While this high voltage is great for transferring power over large distances, the voltage levels aren't usable to consumers. To further distribute power then, the regional grid transforms the voltage down to 66 kV and 132 kV. The regional grid is then further connected to the distribution grid, which, as implied by its name, further distributes power at 11 kV and 22 kV to consumers. Between the distribution grid and the consumers, there are also transformers, which provide the consumer with the appropriate voltage level. For households in most of Europe, the standard voltage level is 230 V, while industry equipment may require more power that requires higher voltages. Worth noting is that the specific naming and ranges of voltages in the power grid may differ between regions and operators [17].

The power grid is intertwined with grids, transformers, and generators which all need to function coherently with each other. A synchronous generator or synchronous motor operates at a given frequency. The frequency of a generator, f, given in hertz, follows

$$f = \frac{np}{120}, \tag{4}$$

where n is the number of revolutions per minute of the generator and p is the number of magnetic poles [18].

Generators deliver power to the grid, which transfers it to loads. In grids, several generators are connected, making them work in unison, i.e., they are synchronised. This synchronisation makes the generators and equipment in the grid operate at a common frequency. When synchronization within the grid is compromised, disturbances can occur, potentially resulting in partial

disconnections or complete blackouts. Generators and equipment that rely on stable frequencies can also start operating incorrectly. The variability in frequency is quantified by the equation (4), where an increase in the frequency necessitates a change in the rotor speed of the generator.

Transformers are also dependent on a stable frequency. Operation outside of their designated frequency will at best lead to reduced performance and increased energy losses. A too high variance can result in the transformers outputting incorrect voltage levels. This again causes the voltage received by devices to be incorrect, which can disturb or damage them.

The likelihood of major incidents occurring in the grid is handled by the use of protective relays and circuit breakers. These safety mechanisms are crucial for safeguarding the equipment and securing grid stability, as they allow for selective shutdown of parts of equipment or parts of the grid.

2.3 Rate of change of frequency

When large power draws or generation is cut out from the power grid, the grid reacts with an increased or decreased frequency. These deviations are not desirable, and it is crucial for the TSOs to be able to measure the frequency, detect large offsets, and counteract them. The change in frequency is found by measuring the rate of change of frequency (RoCoF). Where RoCoF is the time derivative of the grid frequency. The base unit for this measurement is $\mathrm{Hz\,s^{-1}}$. The RoCoF, with respect to time t follows

$$\mathrm{RoCoF}(t) = \frac{df(t)}{dt} = \frac{1}{2\pi}\frac{d^2\phi(t)}{dt^2}, \tag{5}$$

where $\frac{df(t)}{dt}$ is the first derivative of the frequency and $\frac{d^2\phi(t)}{dt^2}$ is the second derivative of the phase angle ϕ [19].

When a RoCoF event occurs, the lowest or highest point the frequency reaches is commonly denoted as the 'nadir' of the event. This is used throughout literature, while some denote the nadir as the bottom point of the frequency and the 'zenith' as the top point. In this thesis, the term nadir will be used for both the lowest and highest points in an event.

The data analysed in this thesis are not continuous variables but discrete ones. When looking at discrete frequency data, the central finite difference method can be used to calculate the RoCoF [20]. The RoCoF, given in $\mathrm{Hz\,s^{-1}}$ follows

$$\mathrm{RoCoF} = \frac{f(t_{i-X}) - f(t_{i+X})}{2T}, \tag{6}$$

where f is the recorded frequency at different times i. X is the incremental steps from i and $2T$ is the time difference of the two recordings [20].

By using values from each side of point i, the central finite difference reduces the error introduced if one uses only forward or backward differences.

2.4 Inertia

In this theory section on inertia, the theory presented closely follows the ENTSO-E report Ref. [11].

When there is a sudden change in the power balance of a grid, the system frequency begins to change. Inertia present in a system mitigates this change by reducing how fast the frequency changes. Inertia in a power system can be analogously seen as mechanical inertia, which is the resistance of a physical object to change its state of rest or motion. In systems, the inertia of rotating generators provides this resistance of change to the frequency by their rotational mass.

Systems with high amounts of inertia reduce the RoCoF by having the rotating masses of generators absorb or release energy. The initial response by the generators gives TSOs time to employ rectifying measures to the frequency.

Contrarily, a system with a low amount of inertia has less resistance to frequency changes. These systems are often high in power sources which inherently do not provide inertia, like wind and solar. The RoCoF in these systems can, therefore, be faster, giving the TSOs less time to act. The inertia constant of a single generator, H, in seconds, follows

$$H = \frac{1}{2}\frac{J\left(\omega_n\right)^2}{S_n}, \tag{7}$$

where J is the moment of inertia of the generator, given in kgm^2. ω_n is the mechanical angular velocity of the rotor, given in rad/s. S_n is the rated apparent power of the generator, given in voltampere, VA [11].

A large grid consists of several generators. Using the inertia provided by each individual generator, one can find the total inertia of all generators in the system, H_{sys}. Which follows

$$H_{\text{sys}} = \frac{\sum_{i=1}^{N} S_{ni} H_i}{S_{\text{sys}}}, \tag{8}$$

where S_{sys} is the sum of all the apparent power for all generators. S_{ni} is the rated apparent power, in voltampere, VA, of generator i. H_i is the inertia constant of generator i [11].

2.5 Swing equation

In this theory section on the swing equation, the theory presented closely follows the ENTSO-E report Ref. [11].

The swing equation is fundamental for describing and analysing a power system. The equation describes the dynamics of the system when considering the generators generated power, consumed power, frequency, nominal frequency, inertia constant, and apparent power. From these parameters, the swing equation for a single synchronous generator can be demonstrated. The inertia, H_i, with regards to the first derivative of the generator frequency, f_i, follows

$$H_i \frac{df_i}{dt} = \frac{f_n^2}{2S_{ni}f_i}(P_{mi} - P_{ei}), \tag{9}$$

where f_n is the nominal frequency, P_{mi} is the mechanical power of the generator, and P_{ei} is the electrical power provided by the generator [11].

In a power grid with numeral generators working in unison, one can sum their parameters, and express the frequency change of the grid in the Laplace domain. The frequency change, Δf, given in Hz, follows

$$\Delta f = \frac{f_n}{S_n(2H_{sys}s + kf_n)}\Delta P, \tag{10}$$

ΔP is the power imbalance in watts. k is the frequency-dependency of loads, and s is the Laplace operator [11].

Examining equation 10, one can observe that changes in generated or consumed power directly affect the frequency. Optimally, one would always want power generation to match consumption. This is not the case for TSOs, as the consumption of power frequently varies, which demands a matched generation. The relationship of the frequency change with generated and consumed is also not linear, as the terms under the fractional line contribute to a smaller Δf. Thus, having larger values below the fractional line is beneficial as it makes the grid more resilient to power imbalances [11].

2.6 Whittaker-Henderson smoother

A smoother process aims to take in a series of data and apply a mathematical method that estimates new fitted data points to the original data. One such smoothing algorithm is the Whittaker–Henderson (WH) smoother, which was first introduced in 1922 by Edmund Taylor Whittaker in the research article "On a New Method of Graduation" [21]. The WH method has recently been expanded on and programmed in Java by Michael Schmid et al. in the scientific article "Why and How Savitzky–Golay Filters Should Be Replaced" [22]. The WH smoother has seen use in statistics and signal processing to reduce noise while preserving the trends of the original data. To achieve this smoothing, the WH method minimises the least squares objective function, which follows

$$\sum_{i=1}^{n}(y_i - z_i)^2 + \lambda \sum_{i=1}^{n-k}(D^{(k)} z_i)^2, \tag{11}$$

where $\mathbf{y} = (y_1, \ldots, y_n)$ represents the original noisy data, $z = (z_1, \ldots, z_n)$ is the smoothed data, $D^{(k)}$ is the k-th order finite difference matrix, λ is the smoothing parameter controlling smoothness, and k is the order of the derivative used in smoothing [22].

After setting up the objective function, a matrix equation (12) is solved to obtain the smoothed data, which follows

$$(I + \lambda D^{(k)^\top} D^{(k)})z = y, \tag{12}$$

where I is the identity matrix, and $D^{(k)^\top}$ is the transposed matrix of $D^{(k)}$ [22].

When implementing the WH smoother, one controls the parameters order, k, and lambda, λ, where k sets the k-th derivative of the data and λ decides the smoothing strength. Setting larger orders of k penalises higher-order changes in the data. While higher λ values will increase the weight of the smoothing penalty, leading to smoother results. Conversely, smaller values of the parameters will lower the smoothing strength and provide results that are closer to the original data. The interested reader can explore the solving of equation (12) via Cholesky decomposition in Ref. [23].

2.7 IEC/IEEE standards

When the frequency is measured in a power grid, it is important that the quality and accuracy of the measurements are of adequate quality. The quality of measurements is set by The Inter-

national Electrotechnical Commission and the Institute of Electrical and Electronics Engineers (IEC/IEEE). Their standards apply to the TSOs in the NSA, and also a range of other countries in the world. One important standard is the one for phasor measurement units. These measurement devices report on synchronized phasor, frequency and RoCoF. An important note is that all measurement devices need to be capable of receiving time from a precise and reliable source. More specifics around the methods can be found in Ref. [19]. Which is the latest and current standard issued by the IEC/IEEE in 2018.

3 Literature review

In this section, a collection of relevant literature is presented and discussed. Both institutionally published and academic papers looking at inertia, frequency, and RoCoF are reviewed.

Inertia and frequency stability are closely linked when accessing the stability of a power grid. It is therefore interesting to look into what organs, such as the European Network of Transmission System Operators for Electricity (ENTSO-E) and Transmission System Operators (TSOs) regard as challenges and solutions when looking towards the future of power grids. ENTSO-E represents the TSOs across Europe and is working to improve cooperation between the TSOs from different countries. The input from TSOs in such an organ should result in good technical and scientific reports. To dig even deeper into the theme of stability, it is also interesting to look at how some TSOs have prepared themselves for the increase in renewable energy production. In addition to this, it is also interesting to look at how the scientific inquiry sees the development of inertia research and renewable energy.

Lastly, the literature review will contain summaries of scientific publications on inertia and RoCoF. These scientific publications look into how different sizes of power grids deal with detecting RoCoF events. Most work examining smaller grids, such as island grids and isolated networks. This contrasts with the size and scale of the NSA. However, while some methodologies used on smaller grids are not directly applicable to the NSA, some could be. The goal is that by the end of the literary review, methods used in other papers can be utilised to find RoCoF events in the NSA.

3.1 State Organs

3.1.1 ENTSO-E – Future system inertia

The report “Future system inertia 2” [11] by ENTSO-E from 2017 aims to forecast low inertia situations and suggest mitigation tools for the Nordic area towards 2020 and 2025. As stated in the paper, “The structural changes identified in the NSA are not unique, and similar changes are occurring in other systems.”[11] With this in mind, ENTSO-E’s goal with this report is to offer suggestions for improvements.

To gain information about various power systems, ENTSO-E sent out a survey to TSOs affiliated with the Nordic area. The survey included questions about the power system of each TSO and its properties. A part of the survey asked about inertia reduction and if there are measures in place to deal with it. Eight of the twelve respondents indicated that the decrease in inertia is a challenge. Three respondents had no present solution, two systems had marked solutions, and six had non-marked solutions. This indicates that low inertia is a concern among the TSOs. But it has not yet become an issue large enough to cause actions from every TSO [11].

In order to predict future inertia in 2020 and 2025, future market scenarios were specified by responding TSOs. To obtain a good forecast, these market scenarios were obtained via a multi-area power-market simulator. This simulator models over 1200 hydropower units and thermal power plants with output over 100 MW in the NSA. The simulator is enabled to calculate

physical flows and restrictions can manually be applied to the grid. According to ENTSO-E, this provides a more realistic production distribution result [11].

The model's performance was evaluated through a simulation based on data from the year 2014. By incorporating backtesting methods and utilizing weather data from the same year, the outputs generated by the model were compared against actual 2014 data. Findings indicated a high degree of accuracy in the model's predictions, with the primary exception being a minor overestimation of hydroelectric production at the lower end of the duration curve.

To ensure that the variations in weather are properly considered, weather data from 1980-2012 are included when the simulation is performed. The results of the simulations indicate that low-inertia situations will occur in 2020 and 2025. With a 99 percentile of kinetic energy being below 120 GW in 2020 and 134 GW in 2025. As the 99 percentile indicates, the system will dip below the specified kinetic energy one percent of the time in a year. From this result, the paper concludes that the limited time of lower inertia does not provide a basis to introduce markets for mitigation purposes.

With this in mind, tools such as Fast Frequency Response (FFR) can still be of use as a correction tool for frequency in general. With the faster response time of FFR, later responding correction tools, such as Frequency Containment Reserves (FCR), automatic Frequency Restoration Reserves (aFFR), and manual Frequency Restoration Reserves (mFFR) are given better conditions for bringing the frequency back to its nominal value [24]. An example of this can be found in the FFR pilot project performed by the Norwegian TSO, Statnett, in 2020 and 2021, where the technical requirements, market conditions, and operating procedures were tested. This pilot project resulted in a commercial market being created for FFR in 2022 [25].

The RoCoF value of an event needs to be 35 $\mathrm{mHz\,s^{-1}}$ or higher to be considered an event. This was found by empirical analysis, as this threshold is not sensitive to frequency filtering methods. The time to reach nadir is also considered, and is found to be between 6 and 15 seconds. This does not mean that events outside of this range cannot happen but that the majority of events are expected to last between 6 and 15 seconds before reaching their nadir value [11].

From the ENTSO-E paper, there seemed to be little concern regarding low inertia for 2020 and 2025. This stems from the high portion of inertia present in the system. This inertia is provided by hydropower and nuclear power plants. However, the proportion of inertia in the NSA is expected to be lower in the coming years due to more power generated by RES.

3.1.2 DNV Report RoCoF

The report "RoCoF - An independent analysis on the ability of Generators to ride through Rate of Change of Frequency values up to 2Hz/s" [26] is written by DNV KEMA for the TSOs of Ireland and Northern Ireland, Eirgrid and SONI. As the title puts it, the goal of the work is to investigate if generators are able to sustain operation through incidents of RoCoF with values up to 2 $\mathrm{Hz\,s^{-1}}$. RoCoF values are accessed from 0.5 $\mathrm{Hz\,s^{-1}}$ to 2.0 $\mathrm{Hz\,s^{-1}}$ in increments of 0.5 $\mathrm{Hz\,s^{-1}}$, with the maximum frequency deviation being set to 1 Hz. This naturally results in RoCoF events having different durations. For example, at 2 $\mathrm{Hz\,s^{-1}}$, the duration of the event would be 0.5 seconds, and at 0.5 $\mathrm{Hz\,s^{-1}}$, the duration is 2 seconds [26]. DNV KEMA used a moving time window of 500 ms when looking for unstable operation during a simulated 1

$\mathrm{Hz\,s^{-1}}$ RoCoF event. This time window duration is in line with other papers like Ref. [27]. Time windows are also adapted as different values of RoCoF are used.

The reasoning behind ordering this report is the expanding integration of more renewable energy sources in the grids of Ireland and Northern Ireland. Both Ireland and Northern Ireland had a goal of hitting 40 percent renewable energy penetration by 2020. As RES decrease the inertia in the grid, it makes RoCoF events more likely to happen.

The results from the study are achieved by simulating generators which are connected to an infinite bus. The simulated generator characteristics are specified by the TSOs, with generator powers ranging from 30 MW to 400 MW. All simulations are run offline and should only be considered as a representation of the real world. The simulation relies on a numerical analysis in a simplified mathematical model. Further details about the methods used are not provided in the report. However, it is clearly stated that the model does not include dampening effects or speed governor action. The work further explains that a fully-fledged simulation could be more accurate [26].

A simulation run with a 500ms time window and a RoCoF of 1 $\mathrm{Hz\,s^{-1}}$ yielded no unstable operation except for a leading power factor. The paper states that this result most likely applies to all generators considered in the simulation. At larger time windows and RoCoF values, unstable operation was detected in the generators.

When experiencing a RoCoF event, generators experience a gain in torque. This is assessed when looking at higher values of RoCoF. The results point to an experienced torque of around 160 percent when the generator is put through a RoCoF of 1 $\mathrm{Hz\,s^{-1}}$. With higher values of RoCoF, this percentage can also be assumed to increase. The time run in this exceeded maximum rated torque state is limited. Comparably the torque can increase to 300–400 percent when there are voltage dips due to generators short-circuiting. Generators can operate after such events, and therefore, they should also be expected to handle RoCoF events causing an increase in torque. An important note made is that the wear on generators could be larger if regular RoCoF events were to occur, but this is not investigated further [26].

3.1.3 Renewables and inertia in Europe

Mehigan et al. (2020) investigate inertia scenarios for the European grid in the scientific publication “Renewables in the European power system and the impact on system rotational inertia” [28]. With the EU setting ambitious renewable power and greenhouse gas emission goals for 2030 and 2050 [4], the scene is set to investigate possible future scenarios regarding inertia and RoCoF. The two scenarios in this paper are based on scenarios by the ENTSO-E Visions for 2030. Information about these scenarios by ENTSO-E can be found in the paper “ENTSO-E Ten-Year Network Development Plan” [29]. In short, the paper depicts different scenarios with demands for electrical energy, variable renewable capacity, CO2 prices, and more in 2030. When choosing to build on the scenarios presented by ENTSO-E in 2016, the paper looks at the most pessimistic outlook, Vision 1, and the most optimistic one, Vision 4. A few key points from these scenarios are electricity demand and variable renewable capacity. The Vision 1 outlook predicts a European energy demand of 3434 TWh of energy and a variable renewable capacity of 388 GW. Vision 4 predicts an energy demand of 3616 TWh and a variable renewable capacity of

614 GW. The difference in renewable capacity is considerable in the two scenarios. And also interestingly the total energy demand is bigger for Vision 4. As ENTSO-E points out, Vision 4 has an increase in electrical equipment. Most notably, Vision 4 includes an optimistic increase in installed heat pumps and electrical vehicles. Which will drive up energy usage from the grid and reduce the energy demand for fossil fuels [28].

With the ENTSO-E scenarios in mind, the paper looks at three new scenarios regarding inertia. One where no minimum inertia criteria are set and two where inertia constraints are set so the RoCoF will not exceed 0.5 $\mathrm{Hz\,s^{-1}}$ and 1.0 $\mathrm{Hz\,s^{-1}}$. These scenarios are put into simulations of existing systems in Europe. The considered synchronous grids were the Baltic grid, the Central European grid, the Great Britain grid, and the Nordic grid. To evaluate scenarios for the given constraints, the largest infeed of power to the systems is set to drop out from the grid. The largest feed of power for the grids is set to the largest producing generator within the grid or a cross-border connection, whichever is larger. The one exception is the central European grid. Where the largest feed of power is set to 3000 MW, representing the failure of two nuclear reactors. This is based on ENTSO-E's definition of 'Reference Incident' in the central European synchronous grid [28].

In this instance, the power systems are examined as a large synchronous machine, with inertia approximated as the sum of each individual generator. The inertia from wind power could be advocated to be included, but it is considered to be zero.

It would be an excess of information to add results from all regions in this thesis. The interested reader can find these in Table 5 at Ref. [28]. Two that will be mentioned are the central European grid and the Nordic grid. With the largest infeed of power of 3000 MW cut out, the central European grid has an assigned minimum inertia of 75 GWs for a RoCoF limit of 1 $\mathrm{Hz\,s^{-1}}$ and 150 GWs for a RoCoF limit of 0.5 $\mathrm{Hz\,s^{-1}}$. The Nordic synchronous with the largest infeed of 1400 MWs has an assigned minimum inertia of 35 GWs for a RoCoF limit of 1 $\mathrm{Hz\,s^{-1}}$ and 70 GWs for a RoCoF limit of 0.5 $\mathrm{Hz\,s^{-1}}$. For the systems to not exceed the RoCoF limit of 0.5 $\mathrm{Hz\,s^{-1}}$, it can be observed that the minimum inertia needs to be doubled. Not surprisingly, the results for the other regions are also linear in this regard. The inertia duration curves can be viewed in Fig. 2.

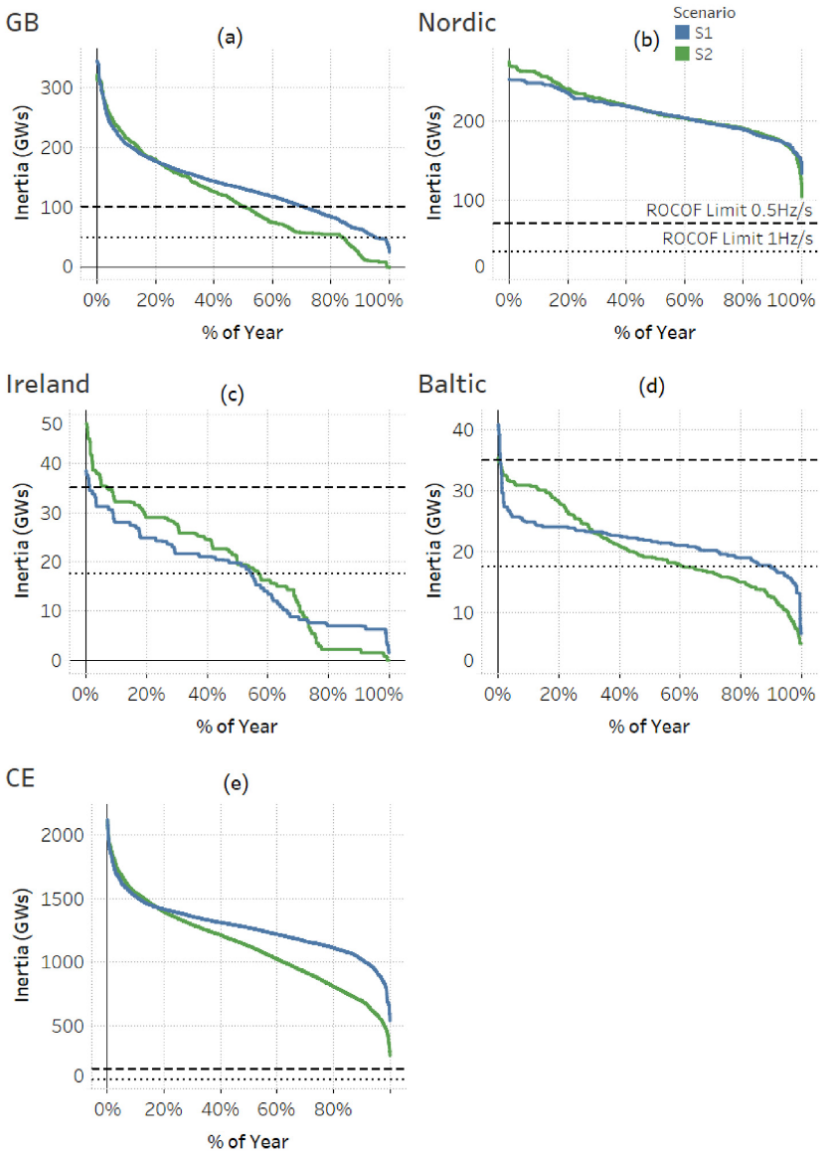

Figure 2: Inertia duration curves for synchronous grids in Europe with no RoCoF limit. The different curves represent 2 separate scenarios, marked in green and blue. The horizontal axis represents the duration, while the vertical represents inertia in GWs. The figure is taken from 'Renewables in the European power system and the impact on system rotational inertia' with permission [28].

On the basis given by ENTSO-E and the simulations run in this paper, the required minimum inertia to avoid RoCoF events of 0.5 $\mathrm{Hz\,s^{-1}}$ is high and is highly variable between different regions. The doubling in inertia requirement from 1 $\mathrm{Hz\,s^{-1}}$ to 0.5 $\mathrm{Hz\,s^{-1}}$ seems unreasonable, and there are no recommended inertia and RoCoF levels that should be set. With a 0.5 $\mathrm{Hz\,s^{-1}}$ RoCoF limit, the system would be more solid with more inertia, but this does not look feasible when most of the RES, which are to be installed, wind and solar, are low in inertia. The solution for a 0.5 $\mathrm{Hz\,s^{-1}}$ RoCoF limit would be to introduce synthetic inertia, flywheels, or increase the number of inertia-contributing power sources. This could provide base levels of inertia at the

cost of small amounts of nuclear waste [28].

3.1.4 Nordic Grid Development

The "Nordic Grid Development Perspective 2023", is a joint report by the Nordic TSOs, Statnett, Fingrid, Svenska kraftnät, and Energinet [30]. The report gives a perspective on the development of the Nordic electricity grid. The most important takeaway points in the report are grid development and flexibility. This is required to happen if the Nordic countries are to reach net zero carbon emissions by 2050. This goal is set by the EU [4], but national binding targets in the Nordic countries are also set towards reaching net zero emissions. This change in carbon emissions requires increased electrical power usage in sectors like data centres, industry, transportation, and heating. According to one scenario, demand is expected to more than double in the next twenty to thirty years. The same scenario predicts a large increase in power production from wind and solar to deal with the increased demand. Also notable is that the traditional power sources in the Nordics, hydro and nuclear, are not expected to have any substantial increase in power production [30].

Another important prerequisite is a reinforced transmission grid. Not only internally for each country but also between the countries in the NSA. In addition to handling more power flow, the grid also needs to be able to handle more distributed power production. This introduction of distributed power production by wind and solar also comes with the added complexity of not having the same stabilizing characteristics as synchronous generators have. Further penetration of RES, therefore, needs to be complimented by electronic or mechanical solutions to maintain the stability of the grid [30].

3.1.5 Fingrid Frequency quality analysis

The report "Frequency quality analysis - 2022", analyses frequency variations in the Nordic Synchronous Area [31]. The report was written and published by the Finnish TSO, Fingrid. The report widely analyses the power-grid frequency of 2022 of the NSA, with the aim of correctly presenting the frequency quality not only for 2022 but also comparing it to previous years. Average frequency, frequency deviation, frequency area and time outside of frequency ranges are all attributed to their own section in the report. More information on these can be found in the report Ref. [31]. Focusing on the average frequency deviation, which is divided into months, days, hours and minutes. The best-performing month regarding average frequency deviation is December, which has a deviation of 37.5 mHz. Following closely to this value are the months of November and July. The worst months are April and May, with average frequency deviations of 42.1 and 42.5 mHz [31].

The day with the lowest average frequency deviation is Sunday, with the value 38.7 mHz. The highest deviation by day of the week can be observed to be Tuesday, with the average deviation being 41.7 mHz. The average frequency deviation for the hours are highest from hour 23–07, being above 40 mHz for these hours, except for hour 6, when the deviation is 38.6 mHz. The lowest deviation in hours is found at 14, with an average value of 36 mHz.

The minute resolution focuses on minutes of the hour for the whole year. Results show that

the frequency deviation for 2022 is highest at the start of hours. With the standard deviation breaching 50 mHz in the first minute of the hour. The lowest deviation can be found at minute 29, and the overall average value is found to be just above 36 mHz. For the interested reader, the full figures explaining the average frequency deviation can be viewed on pages 11–18 at Ref. [31].

Towards the end of the report, larger disturbances in the frequency are addressed. To be considered a disturbance, the nadir needs to exceed 300 mHz, and the incident also need to have an initial frequency gradient over 0.035 $\mathrm{Hz\,s^{-1}}$. With these restrictions, there were 16 larger disturbances in 2022. With 9 being related to nuclear power generation, 6 being related to HVDC, and 1 being AC-line related. For the interested reader, more specifics around each of these events can be found on pages 101–120 at Ref. [31].

The report concludes that the frequency quality of 2022 was better than in the preceding year. Notably, this is concluded with the amount of oscillation and disturbances over 300 mHz being disregarded. With the years 2017–2020 having an average of 6 larger deviations, the 2022 number of 16 is a substantial increase. This indicates an increasing trend in larger disturbances.

3.2 RoCoF and filtering methods

3.2.1 The Hawaiian grid

He Yin et al. (2022) look at the grids of the Hawaiian islands in the scientific paper "Precise ROCOF estimation algorithm for low inertia power grids" [27]. Real-world frequency data are measured at a sampling rate of 120 Hz from June 11, 2021 to August 8, 2021. The recordings are performed at two locations, on the islands Maui and Kauai.

The paper aims to improve a method for standard RoCoF estimation method based on differences in adjacent frequency measurements. This method is susceptible to noise from real-world recordings. To overcome this, the paper offers an estimation based on the least-squares method with changeable time windows. It is stated that larger time windows of 0.1 to 0.5 seconds are generally used for high inertia grids. For low-inertia grids like the Hawaiian, time windows cannot be too big, as breaker operations and noise can trigger a RoCoF event detection. This is because of the low inertia that poses a lower arresting time, i.e., the time before the frequency reaches the nadir. Therefore, the detection needs to be quicker for a low inertia grid, than for a large grid with high inertia.

Offline calculations done on the RoCoF estimation are treated as ground truth. This is then compared to the calculations done online. These calculations show that the online calculations can follow the offline calculations. Based on the analysis in the paper, time windows of both 0.05 and 0.3 seconds are evaluated when performing the RoCoF estimations. Both of these time windows are able to capture long arresting and hybrid arresting events. It is emphasised that the 0.05-second window is useful when a short response time is desired in the Hawaiian grid. Using a median filter to filter out frequency spikes that cause transient events is also advocated. As the aim of this paper is to find long arresting periods and hybrid arresting events [27]. The offline vs. online calculations performed are illustrated in Fig. 3.

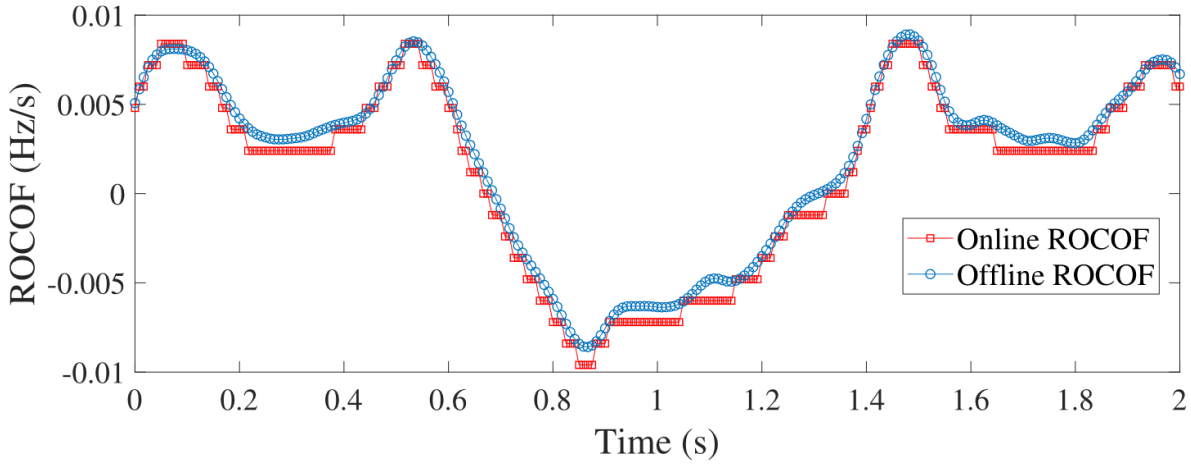

Figure 3: RoCoF estimation comparison between online and offline calculation. The vertical axis shows RoCoF values, and the horizontal axis shows time. This figure is taken from the paper 'Precise ROCOF estimation algorithm for low inertia power grids' with permission [27].

While offline calculations are more precise, as Fig. 3 clearly illustrates, online calculations can be nearly as precise as offline ones. Even though the Nordic grid is much larger than those in Hawaii, the least-squares and median filter methods are still applicable, as they offer better precision and estimation of RoCoF events [27].

3.2.2 Smoothing discrete continuous data

Michael Scmid et al. (2022) look into why the Savitzky-Golay filters should be replaced in the paper "Why and How Savitzky-Golay Filters Should Be Replaced" [22]. This paper looks at improvements and replacements to the Savitzky-Golay (SG) filter, which was first popularised in the mid-1960s. The SG method is based on local least-squares fitting of data by polynomials. To improve the SG filter further, it is proposed to add weights to the method. Added weights, when smoothing with the SG filter, would reduce the impact of data points at the edges of the data. Where the SG method is known to experience inaccuracies. The authors have chosen Hann-square weights to improve the SG filter. The weighted SG is given the abbreviation SGW. Two other filters are also considered: the modified sinc kernel (MS) and the Whittaker–Hendeson (WH). Where the MS filter is based around the sinc (sin x/x) function with a Gaussian window, and the WH filter tries to minimize the sum of squared differences while incorporating a penalty term which can be tuned to balance smoothness. All the different filters are evaluated on their performance in smoothing sine waves and a series of Gaussian peaks with successively smaller widths.

After running the smoother on a variety of data and with different filter parameters, the paper finds that the SGW outperforms the SG filter by supplying weights to its polynomial fit. However, the filters, MS, and WH further outperform the SGW. A notable improvement is in the handling of boundary and near-boundary values. Where the MS and WH offer better smoothing. In overall smoothing capability, the WH filter performs well but is surpassed by the MS filter. The MS filter showed fewer artefacts and an even better handling of edge values than

the WH.

This comes at a cost, with the MS filter combined with linear extrapolation of data requiring higher computing resources. This should be taken into consideration when choosing a filter. For a smaller dataset, the MS filter would yield great results with a limited computing time due to the amount of data being handled. For bigger datasets, the MS filter could also be a possible choice. This is if the smoothing of data is required to be as precise as possible or if one has the computing power available. However, if the smoothing needs to be satisfactory, but not excellent, the WH filter should be considered. When looking at the results presented, the WH filter handles peak values and edge values better than SG and SGW. Even when compared to the better-performing MS filter, the WH filter still provides adequate smoothing [22].

4 Methodology

The methodology section contains information on the dataset used for the thesis and the methods employed for cleaning and analyzing the data. After processing the data, the goal is to identify and organise RoCoF events within the NSA systematically. All data processing is carried out in Python. Where several packages have been utilised to perform the cleaning, analysis, and plotting. Some of these are numpy [32], pandas [32], multiprocessing [33, 34], matplotlib [35], and seaborn [36]. The Python code for analysis has been written in the process of writing the thesis, and the code is incorporated with parameters to enable further utilisation of the code and the underlying logic. The analysis and plotting scripts can all be found on GitHub at Ref. [37]. The flowchart in Fig. 4 displays the workflow when handling the data.

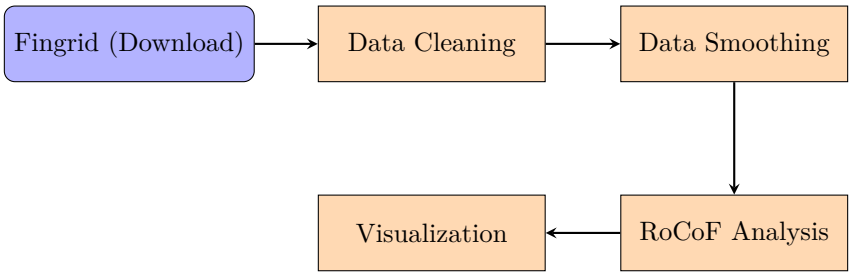

Figure 4: This flowchart sketch displays the workflow of the analysis. First, the data is stored by individually downloading zipped files from Fingrid [9]. The data is then cleaned, and missing values are identified and forward-filled. The smoothing process then employs a Whittaker–Henderson filter with a lambda value of 4 and an order value of 2. Afterwards, a RoCoF analysis is performed, looking for RoCoF events with a minimum RoCoF value of 40 $\mathrm{mHz\,s^{-1}}$ and a minimum nadir value of 35 mHz. Lastly, the data is visualized using matplotlib and seaborn.

4.1 Power-grid frequency dataset from Fingrid

The dataset utilised in this thesis is sourced from the Finnish TSO, Fingrid, and is licensed under the Creative Commons Attribution, allowing for unrestricted use [9]. Power-grid frequency measurements were conducted with a sampling rate of 10 Hz, i.e., ten measurements per second, and were recorded at various undisclosed 400 kV substations within the Finnish grid. The devices used to measure the frequency are called phasor measurement units. These devices are ensured to adhere to the latest IEEE standards. These standards are regularly updated and given in preceding order as IEEE 60255-118-1:2018 [19], IEEE:C37.118.1-2011 [38], IEEE:C37.118.1a-2014 [39], IEEE C37.118 [40].

These standards are in place to make sure that Fingrids' time and frequency measurements are recorded with adequate precision. The information regarding standards used by Fingrid was obtained through email communication with Fingrid [41].

Fingrid organizes its frequency datasets by month and offers them as zipped files. In later years, the format used has changed from '.zip' to '.7z'. Having all zipped files in the same format is desirable, so all .7z files have been repacked into .zip files. Within the monthly files, individual '.csv' files contain data from each day of the month, including a time column giving precise

timestamps of the frequency measurements. The timestamps follow UTC+2 or UTC+3, varying by daylight saving time. The total length of the data analysed is from the 1st of January 2015 to the 31st of 2023. There are no months stripped of recordings, but missing data are present in the dataset. The total size of the zipped dataset is 9.26 GB, which, with a compression rate of around 9, equates to 83.3 GB of data.

4.2 Data cleaning

The code used for data cleaning is built on top of already existing code to explore a frequency dataset, which was provided by the supervisor for this thesis, Leonardo Rydin Gorjão. The code which was provided is named 'Base filtering.py' and can be found at Ref. [37].

The files obtained from Fingrid are organised locally into yearly folders and are separated from subsequently created folders to avoid overwriting data and maintain integrity. Python code is then employed to read and compile individual daily files into a single .csv file representing an entire month. In this assembly process, the frequency also undertakes a transformation wherein 50 Hz is subtracted from the frequency column and then multiplied by 1000, thereby shifting the reference frame to 0 mHz. This adjustment proves advantageous, particularly given that frequency variations within large systems like the NSA tend to be minimal. This reference frame also makes it easier to compare results with grids with differing nominal frequencies. Moreover, examining the data in mHz enhances clarity when conducting further analysis. Given that subsequent processing methods require a continuous data series, it is imperative to verify the integrity of the raw data. This verification is accomplished through specific lines of code, documented within the 'Data filtering.py' file, which can be found at Ref. [37].

```
#....
# Create rows for missing 0.1-second intervals.
df_resampled = combined_df.resample('0.1S').asfreq()

# Column to show whether the 'Frequency' value is NaN.
df_resampled['filled'] =
df_resampled['Frequency'].isna()

# Forward filling with previous valid value.
df_resampled['Frequency'] =
df_resampled['Frequency'].ffill()

# Total number of times forward filling has happened.
total_fill_count = df_resampled['filled'].sum()
#....
```

- The first line of code facilitates data resampling, generating new entries for time intervals where date and frequency measurements are absent.
- Subsequently, the second line introduces a new column, `filled`, indicating the presence of added rows. This is achieved by assessing whether the frequency column in a given row contains a NaN (Not-a-Number) value, indicating a missing frequency measurement.
- Next, the third line employs forward filling to populate frequency data in rows lacking

measurements, utilising only existing raw frequency values for this purpose. Importantly, forward filling occurs exclusively in rows that are missing frequency values.

- Finally, the last line counts the number of NaN values in the `filled` column, reflecting the number of forward-filling occurrences. This count serves as a basis for calculating the percentage of missing values in the dataset for the month, as depicted in Fig. 5.

Following these steps, the processed data is prepared for subsequent analyses. It is archived in a zipped format, and stored in a new location. This precaution safeguards data integrity and ensures the utilisation of the correct data in subsequent steps.

The missing data for the dataset is graphically represented in Fig. 5.

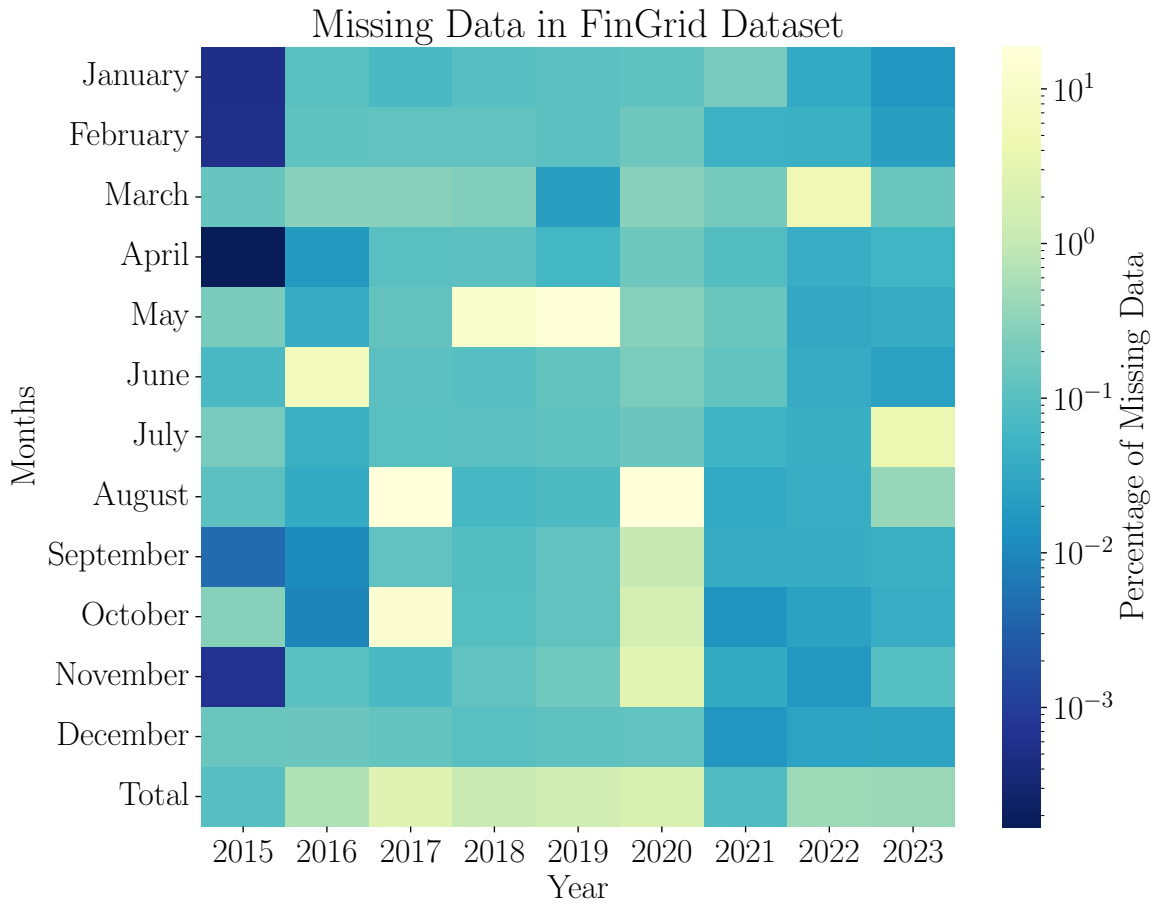

Figure 5: The heatmap shows the logarithmic percentage of missing data in the Fingrid frequency dataset. The vertical axis displays the month of the different years and also includes a row for the total of the years. The horizontal axis represents the year. A lighter color illustrates months with more missing data, while a darker color indicates less missing data. The worst month is August of 2017, with 18.62 percent missing data. The best month is April of 2015, which has 0.00017 percent missing data. The total missing data from 2015–2023 is around 1 percent.

The logarithmic scale of the coloured bar reflects the highly variable percentage of missing data. Overall, approximately 1 percent of raw data is missing. With the best month exhibiting a mere 0.00017 percent missing data. While months with less available data may conceal RoCoF events, such occurrences are inevitable. However, given the generally high quality of the data, this concern is relatively minor.

4.3 Smoothing data

Smoothing the frequency data is a crucial step in preparing for the identification of RoCoF events. This process reduces noise and mitigates outliers present in the dataset. Various methods exist for smoothing a data series, with a key consideration being tunability. This is crucial when one wants to strike the balance between smoothing out noise and not excessively smoothing the data. Overdoing the smoothing might diminish the intensity of RoCoF events or could lead to them going undetected. The Whittaker-Henderson smoother offers excellent tunability features. The original code is written in Java and can be found under 'Supporting Information' in the paper "Why and How Savitzky-Golay Filters Should Be Replaced" [22]. To work in a Python environment for usage in this thesis, the code has been translated from Java to Python. The file containing the class for this smoother can be found in the file 'WhittakerHendersonSmoother.py'. The code employing the smoother is found in the file 'Smoothing using Whittaker-Henderson.py'. Both are made available at Ref. [37].

The Whittaker-Henderson smoother incorporates the parameters, `order` and `lambda` to govern its behaviour. The `order` parameter determines the degree of penalty applied to derivatives during smoothing, with higher values imposing greater penalties on higher-order derivatives. Meanwhile, the `lambda` is a regularisation parameter, striking a balance between fitting and smoothness. To choose optimal parameters, one could use cross-validation. This is not performed, as a visual inspection of the smoothing was deemed sufficient. Extensive information on using cross-validation when using a WH smoother can be found in the article 'A Perfect Smoother' [42].

Smoothing large amounts of data demands significant processing power, resulting in considerable time usage. A limiting factor in this regard is Python's Global Interpreter Lock (GIL) [43], which restricts concurrent access to data by allowing only one Python instance to execute code. While this mechanism minimises the risk of data corruption, ensures thread safety, and makes single-threaded processes faster, it also restricts multiprocessing. The usage of the numpy package is also a limiting factor regarding processing time. As it is not very efficient at handling matrices. A possibility could have been to perform the smoothing in Matlab, which is shown to outperform numpy in the article Ref. [44].

To address the processing power limitation, the multiprocessing package is employed to divide the whole data frame into smaller data frames called chunks. This allows multiple processing threads to work on chunks of the whole dataset in parallel. Although this approach enhances processing time, it may lead to uneven smoothing at data breakpoints. Here, it is worth noting that the Whittaker-Henderson smoother nicely managed to smooth data even at breakpoints.

Multiprocessing significantly increases memory usage, as each GIL instance gets allocated

its own memory space and accesses chunks of the whole data frame simultaneously. This may cause computer memory to be a possible limitation. The following code from 'Smoothing using Whittaker-Henderson.py' highlights how multiprocessing is executed.

```
from WhittakerHendersonSmoother import WhittakerHendersonSmoother
from multiprocessing import Pool
#....
def smooth_data(chunk, order, lambda_val):
    smoother = WhittakerHendersonSmoother(len(chunk)
                                          , order, lambda_val)
    return smoother.smooth(chunk)

if __name__ == '__main__':
    order = 2
    lambda_val = 4
    frequency_data = df['Frequency'].values

    # Split data into chunks
    chunk_size = 10000
    chunks = [(frequency_data[i:i + chunk_size],
               order, lambda_val)
    for i in range(0, len(frequency_data),chunk_size)]

    # Process pool to smooth the chunks in parallel
    with Pool(3) as pool:
        smoothed_chunks = pool.starmap
                          (smooth_data, chunks)
#....
```

- The function `smooth_data` is designed to handle chunks of the total data frame by instantiating the Whittaker-Henderson smoother on each individual chunk.
- Following this function, a condition ensures that certain code only runs when the script is executed directly, not when it is imported as a module. Subsequently, the script defines the values for `order` and `lambda` parameters. The `order` is set to 2, as this enables the smoother to penalize high variations in the data. The lambda parameter is found to provide satisfactory results at a value of 4. The script then extracts frequency values from the data frame, `df`.
- In the subsequent section of the code, the frequency data is divided into chunks, with the size of each chunk determined by the variable `chunk_size`. These chunks are created in increments of ten thousand and, combined, cover the entire range of the total data frame.
- Finally, the script creates three pools to manage the chunks generated. Utilizing the `smooth_data` function, these pools handle the chunks in parallel and return the smoothed data. This smoothed data is then later combined alongside the original raw frequency measurements.

The resulting smoothed frequency data is satisfactory, and is displayed in Fig. 6 alongside the original raw frequency and a RoCoF calculation.

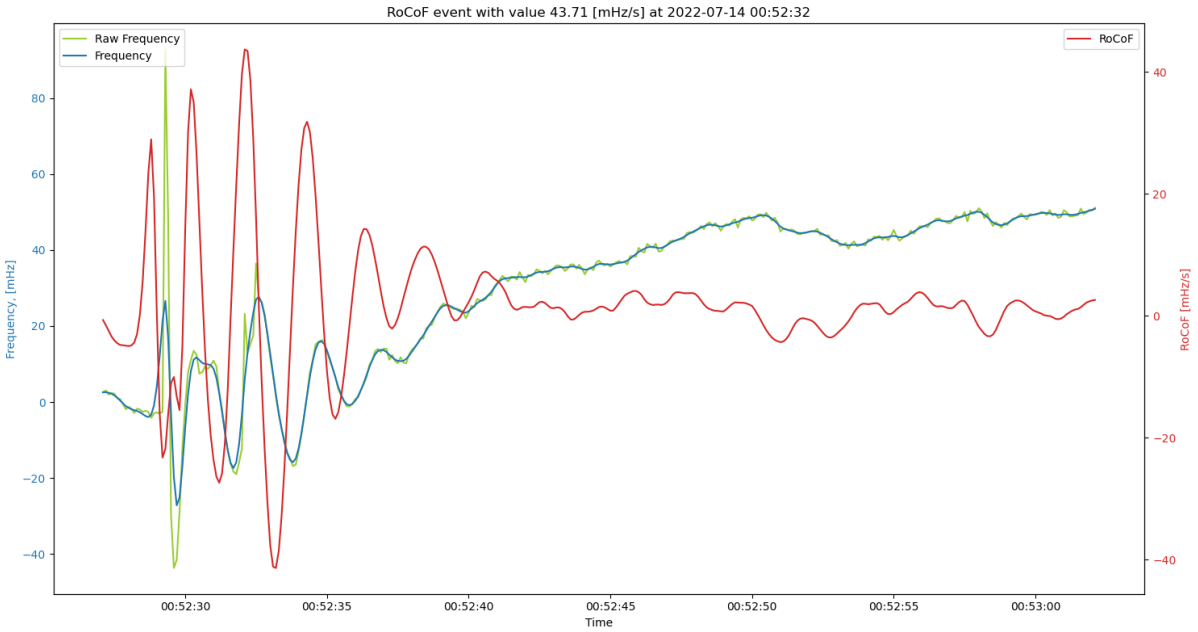

Figure 6: The impact of the WH smoother is displayed, with the horizontal axis showing the time and the dual vertical axis displaying frequency and RoCoF values. The original frequency is shown in green, the smoothed frequency data is represented in blue. The red line displays the calculated RoCoF.

Examining Fig. 6 shows that the smoother operates as expected with an order of 2 and a lambda of 4. It reduces the highly variable frequency values which are present at the start of the event, while preserving the original trends.

4.4 RoCoF Analysis

To calculate the RoCoF values of the smoothed frequency data, equation (6) is utilised. The RoCoF value for each point in time is calculated by shifting five values backwards and forwards, subtracting the values found, and then dividing by the time between the points. The only RoCoF values that can not be obtained are those closer than five rows to the edges of the data frame. Since the data is divided into months, some RoCoF values are unobtainable. This is a drawback but is not expected to cause any issues.

To be considered an event, the RoCoF value needs to exceed 40 $\mathrm{mHz\,s^{-1}}$. If no limit were set, even a small change in the frequency would cause the detection of an event. Notably, the value limit chosen for RoCoF in this analysis is 5 $\mathrm{mHz\,s^{-1}}$ greater than the RoCoF limit used by ENTSO-E. The details regarding this limit by ENTSO-E can be read on pages 21 and 22 in the report Ref. [11]. The main argument by ENTSO-E for choosing 35 $\mathrm{mHz\,s^{-1}}$ as a threshold is that event starts were not seen to be affected by frequency filtering. In hindsight, the threshold used in this thesis should have matched ENTSO-Es. However, the limits are proficient, as RoCoF events of higher severity are identified. The code below shows how the RoCoF events were found

and identified. It is available in the script 'RoCoF analysis.py' at Ref. [37].

```
#....

def calculate_rocof(N, T, rocof_limit,freq_change_limit,year,month):

    # Calculate the RoCoF using the symmetric difference quotient.
    df['rocof'] = (df['Frequency'].shift(-N) - df['Frequency'].shift(N)) / (2 * T)

    #Identifying rocof_event and event_start
    df['rocof_event'] = np.abs(df['rocof']) > rocof_limit
    df['event_start'] = (np.abs(df['rocof']) > rocof_limit)
#....

N=5                         # number of data points to shift.
T=0.5                       # time of the total shift.
rocof_limit = 40            # minimum RoCoF value to be considered an event.
freq_change_limit = 35      # minimum change in frequency to be considered an event.
df_rocof = calculate_rocof(df, N, T, rocof_limit,freq_change_limit).copy()
#....
```

- At the end of the code, the parameters N, T, and `rocof_limit` are defined. They are set to `N=5` and `T=0.5`. The code looks 5 recordings backwards 5 forwards and then divides by the time between them. Thus finding the RoCoF of a specific point. Given that Fingrid utilises a recording rate of 10 Hz, shifting 5 points forward and backward results in a time span of 1 second between them, giving $T = 0.5$.
- Then the `calculate_rocof` function is called with these parameters to compute RoCoF for the provided DataFrame, `df`. The resulting DataFrame with RoCoF events are marked and stored in a new column called `df_rocof`.
- After all RoCoF values have been calculated the code marks recordings that exceed the limit of 40 mHz s^{-1}. This is of use when separating and defining what range of data an event should contain.

Marking an event's start is necessary to distinguish and examine the events individually. By marking the start and keeping values surrounding the event start as `part_of_event`, useful data is identified appropriately. The logic of the code is set to mark an event start when the RoCoF value is greater than 40 mHz s^{-1}. This needs to be done only at the start of an event and not for RoCoF values inside the event. Which are likely to have RoCoF values exceeding the threshold. Logic is applied in code to correctly mark the range of an event by introducing a cooldown to the marking of `event_start`.

```
#....
    # Initialize cooldown
    cooldown = 0

    # Initialize part_of_event column
    df['part_of_event'] = float(False)

    for i in range(len(df)):
        # If a RoCoF event is found and the cooldown period has ended
        if df.loc[i, 'rocof_event'] == True and cooldown == 0:
```

```
11              # Start the cooldown period
12              cooldown = 60 * N
13              # Set event_start to True
14              df.loc[i, 'event_start'] = True
15              # Set part_of_event to True for 10*N rows before and 60*N rows after the event
16              df.loc[max(0, i - 10 * N) : i - 1, 'part_of_event'] = float(True)
17              df.loc[i : i + 60 * N, 'part_of_event'] = float(True)
18
19              # Set event_start to True
20              #df.loc[i, 'event_start'] = True
21          elif cooldown > 0:
22          # If in the cooldown period, suppress any RoCoF events
23              df.loc[i, 'rocof_event'] = False
24              df.loc[i, 'event_start'] = False
25              #cooldown -= 1
26          # Decrement the cooldown counter at each iteration
27          cooldown = max(0, cooldown - 1)
28
29      # Drop rows where RoCoF event is False
30      df = df[df['part_of_event'] == True]
31      # Reset the index
32      df = df.reset_index(drop=True)
33  #....
```

- The cooldown of marking an event is initially set to 0. Earlier in the code, a value was set in the column `rocof_event` if the RoCoF value exceeded 40 mHz s^{-1}. This is now used as a marker. The code detects the first row where the `rocof_event` is True (it has a value).
- Afterwards, a cooldown is started, and the column `rocof_event` is set to True. A column called `part_of_event` is then filled with float (True) statements for the rows that should be included in the event. In this case, 50 rows before and 300 after the event starts are included in the `part_of_event`. The recordings are done at 10 Hz, which makes 5 seconds before the `event_start` and 30 seconds after being included and marked as `part_of_event`.
- After the first RoCoF event is detected, the cooldown is set to 300. This makes it so that another event cannot be marked for the next 300 rows, or 30 seconds after an event starts. A drawback of such an approach is that subsequent events caused by the main event could be missed. However, since the data inside the event is kept as a part of the event, these values are still saved.
- After going through the data frame, the code only keeps rows where the `part_of_event` column is True. At the end of the code, the data frame now consists of 6 columns. They are: `Time`, `Frequency`, `Raw_frequency`, `rocof`,`rocof_event` `event_start` and `part_of_event`. These values will be used to find the maximum RoCoF inside an event, the nadir, and the time it took before reaching the nadir.

The nadir of an event is of particular interest as it reveals the maximum deviation in frequency, with the reference point being the frequency at the start of the event. This can easily be observed when looking at individual events. How to solve this in code is not that obvious. The chosen method is to look for absolute maximum or minimum values of frequency inside an event.

The reference point for this deviation is calculated as the mean of the three frequency values prior to the event start. A limit is also applied to the nadir value. If an event does not exceed a deviation of 35 mHz, the event should be removed from the final data frame. The maximum RoCoF is also of interest as it highlights the maximum change the grid was exposed to. All of these steps are executed by the following code,

```
    #....
    # Find the maximum RoCoF value within the event
    max_rocof_idx = df.loc[i : min(i + 60 * N, len(df)), 'rocof'].abs().idxmax()
    df.loc[i, 'max_rocof'] = df.loc[max_rocof_idx, 'rocof']
    #....
    for i in range(len(df)):
    # If a RoCoF event is found
        max_diff = 0
        if df.loc[i, 'rocof_event'] == True:
            if df.loc[i, 'event_start'] == True:
                # Set start_freq at the start of an event
                start_freq = df.loc[i, 'Frequency']
                    # Shift the frequency
                for j in range(i, min(i + 60 * N, len(df))):
                    df.loc[j, 'Shifted_Frequency'] = df.loc[j, 'Frequency'] - start_freq

            avg_prev_freq = df.loc[max(0, i - 3) : i - 1, 'Frequency'].mean()

        # Calculate difference between avg_prev_freq and min_freq_event and max_freq_event
            min_freq_event = df.loc[i : min(i + 60 * N, len(df)), 'Shifted_Frequency'].min
                ()
            max_freq_event = df.loc[i : min(i + 60 * N, len(df)), 'Shifted_Frequency'].max
                ()
            min_diff = abs(avg_prev_freq - min_freq_event)
            max_diff = abs(avg_prev_freq - max_freq_event)
            max_diff = max(min_diff,max_diff)
    # Decide which of the max or min freq event is the biggest
    if abs(min_freq_event) > abs(max_freq_event):
    min_freq_event_idx = df.loc[i : min(i + 60 * N, len(df)), 'Shifted_Frequency'].idxmin
        ()
                print(min_freq_event_idx)
                df.loc[i, 'nadir'] = df.loc[min_freq_event_idx, 'Frequency']
                df.loc[i, 'nadir_time'] = df.loc[min_freq_event_idx, 'Time']
    else:
                max_freq_event_idx = df.loc[i : min(i + 60 * N, len(df)), '
                    Shifted_Frequency'].idxmax()
                print(max_freq_event_idx)
                df.loc[i, 'nadir'] = df.loc[max_freq_event_idx, 'Frequency']
                df.loc[i, 'nadir_time'] = df.loc[max_freq_event_idx, 'Time']

    # Check if the maximum difference is greater than or equal to freq_change_limit
    if max_diff < freq_change_limit:
                freq_limit_rows_to_remove.extend(range(max(0, i - 10 * N), i))
                freq_limit_rows_to_remove.extend(range(i, min(i + 1 + 60 * N, len(df))))
    df = df.drop(freq_limit_rows_to_remove)
    #....
```

- First, the maximum RoCoF inside of the event is located and stored as a column, `max_rocof` in the row where the event started. This makes it easy to locate and use event-specific data.
- The code then searches for places in the data frame where `rocof_event` and event_start

are True, confirming that this specific point in the data frame is an event starting point.

- The code then sets a start frequency, `start_freq`, which is the mean of the three frequency recordings that precede the event start. With the `start_freq` as a reference, the frequency values in the event are shifted. This is necessary because nadir is defined as the deviation from the start of an event. Also notable is that looking at RoCoF events that start with positive or negative frequency values would cause the code to missmark the nadir. Therefore, using the event's start as a reference point is crucial. Afterwards, the code locates the minimum and maximum values of the `Shifted_Frequency`.

- After this, the code chooses which of the minimum or maximum nadir has the greatest absolute value. The greatest of these values is chosen as nadir. The time when nadir was reached is also added in the row of the event start as a column, `nadir_time`. This is later used to calculate how long it took for the frequency to reach its nadir point. An important note here is that it is the original frequency values that are placed into the events start column, not the `Shifted_Frequency`. It is just used as a marker to find nadir.

- Following the calculation of the nadir values, the code checks that the limit denoted `freq_change_limit` is satisfied. This is a limit for the frequency deviation needed for an event to be further analysed. The limit is set to 35 mHz, and events that do not have a deviation larger than this are removed.

Using the minimum and maximum functions to look for nadir has a clear drawback. In some cases, the frequency fluctuates after an event has passed. This may cause the last part of data in an event to be marked as nadir. Even if the event lasted only, say, 5 seconds, the frequency may have changed so much that nadir is marked towards the end of the event window, resulting in it being incorrectly marked.

Since parts of the completed data series are forward-filled,i.e., missing values are replaced by previous ones, there are cases where false RoCoF events are detected. This is due to forward-filled values ending and real values appearing. Forward-filled values, naturally, always follow the same value. When a real value appears after forward-filled values, the RoCoF calculations show a rapid shift in frequency. These events are artificial and need to be excluded. This is performed by the following code,

```
    #....
    ff_rows_to_remove = []
    # Checking forward filled events.
    for i in range(len(df)):
        if df.loc[i, 'rocof_event'] == True:
        # Look at the previous 10*N rows in the raw_frequency column
            raw_frequency_values = df.loc[max(0, i - 10 * N) : i - 1, 'Raw_Frequency']
        # Check if all values are the same
            if raw_frequency_values.nunique() == 1:
            # Add the indices of the rows to be removed to the list
                ff_rows_to_remove.extend(range(max(0, i - 10 * N), i))
                ff_rows_to_remove.extend(range(i, min(i + 1 + 60 * N, len(df))))
                df = df.reset_index(drop=True)
    #....
    df = df.drop(ff_rows_to_remove)
```

```
16      #....
```

- First, an empty list is created. The code then looks for equal values in the previous ten rows of `Raw_Frequency`. If they are equal, the rows for the whole event are added to the empty list for removal, effectively removing the event.
- This handles forward-filling cases before the event. An equal logic is also applied to check for forward-filled cases inside the event. There is a non-zero possibility that the `Raw_Frequency` is consistent in the 10 previous rows while also not being forward filled. This is a minor concern, and when working with the data, no mishaps were found.

Lastly, the 'time-to-nadir' is calculated, which is the time it took from the event starting until nadir was reached. Notably, this parameter was found to be of interest at later stages in the analysis. The code is, therefore, not running in the 'RoCoF analysis.py' file but rather directly in the plotting functions. Because of this, the time-to-nadir is calculated each time a figure is plotted. Since the variable isn't needed before plotting, there is no problem with this approach.

```
1       event_df['time_to_nadir'] = (event_df['nadir_time'] - event_df['Time']).dt.
            total_seconds()
2       event_df = event_df.loc[event_df['time_to_nadir'].between(2, 25)]
```

- The time-to-nadir is calculated by taking the time when the nadir is reached and subtracting it from the start time of the event. The event data frame `event_df` is then updated only to include events which have time-to-nadir values between 2 and 25 seconds. This is done because events with too large or small time-to-nadir values are considered invalid.

4.5 Visualization

The visualization of the results is achieved using the Python libraries matplotlib and seaborn. Matplotlib is used to plot histograms, scatterplots, and individual events, while seaborn is utilized for generating heatmaps. The code used for the visualisation can all be found in the folder 'Plotting' at Github [37].

4.6 Use of artificial intelligence

Generative artificial intelligence (AI) has been on the rise in the past year. It is a powerful and useful tool, which should also be used with caution. Guidelines at NMBU when this thesis is written state that AI tools are allowed to be used if it is done in an ethical and responsible way. Following these guidelines, AI tools have been utilised to improve elements of the analysis and writing. The specific tools used are Grammarly [45], ChatGPT [46], and GitHub copilot [47].

5 Results

The results section covers findings after analysing frequency data from the Finnish TSO, Fingrid [9]. All results are generated using the code described in the method section. In short, the data downloaded from Fingrid are cleaned, the frequency is smoothed, and a RoCoF analysis is performed on frequency data from 2015–2023. All figures in the results section are created with the same datasets. Notably, 204 events have been removed from the results during the analysis. This is done because 'time-to-nadir' values for these events were found to be too low or high. Results with the removed data included can be found in the Appendix, in Fig. A.1–A.5. The code used to generate the results can be found on GitHub at Ref. [37].

5.1 Yearly, hourly and monthly distributions

This subsection contains histograms and a heatplot, which displays in what year, time and month events are occurring. The first histogram shown in Fig. 7 shows event occurrence by year. The second histogram in Fig. 8 separates events by hour. Finally, the last Fig. 9 displays in which month of the year the events occurred.

Examining the total number of RoCoF events within a year can offer insight into the stability of the power system. The histogram in Fig. 7 illustrates the yearly distribution of RoCoF events from 2015 to 2023. Events have been categorised based on the maximum RoCoF found in the event, starting from 40 mHz s^{-1} and increasing at 60-unit intervals. The exact number of events in each range can be found in Table A.1 in the Appendix. Measures are taken to avoid duplicate counts of events ending or starting exactly at intervals.

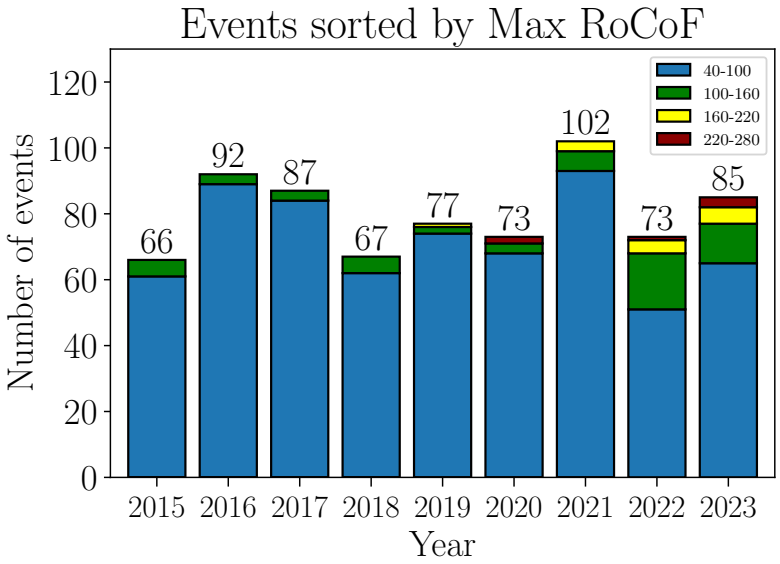

Figure 7: Number of RoCoF events in each year from 2015–2023 in the Nordic Synchronous Area. The number above each bar is the total number of events for the years displayed along the horizontal axis. The events are further sorted by colour, with the maximum RoCoF values detected within each event falling within a RoCoF range, which is given in mHz s^{-1}. The increments are displayed in the legend.

Upon examining the histogram, it is clear that the total number of events does not increase over time. And there seems to be no discernible trend from the total event counts alone. However, notably, the severity of events appears to have increased in later years. Specifically, from 2019 to 2023, there is an increase in events falling within the higher RoCoF ranges. In the range 220-280 mHz s^{-1}, there were three events in 2023, one in 2022 and two in 2020. For the range 160-220 mHz s^{-1}, there are five events in 2023, four in 2022, three in 2021, and one in 2019. A big increase in events that fall into the range of 100-160 mHz s^{-1} for 2023 and 2022 can also be observed. Compared to previous years with between two and six events in this range, 2022 had seventeen, while 2023 had twelve.

Another interesting statistic is the time of occurrence for the events. This could provide insight into at what times of the day events have been most likely to occur. This is displayed in Fig. 8. The histograms are sorting events based on the time of occurrence. The large histogram is created with data from 2015–2023, while the subplots contain yearly data. The events are placed based on the starting hour. As an example, an event which occurred at hour 06:59, would be placed in the hour 6 bar.

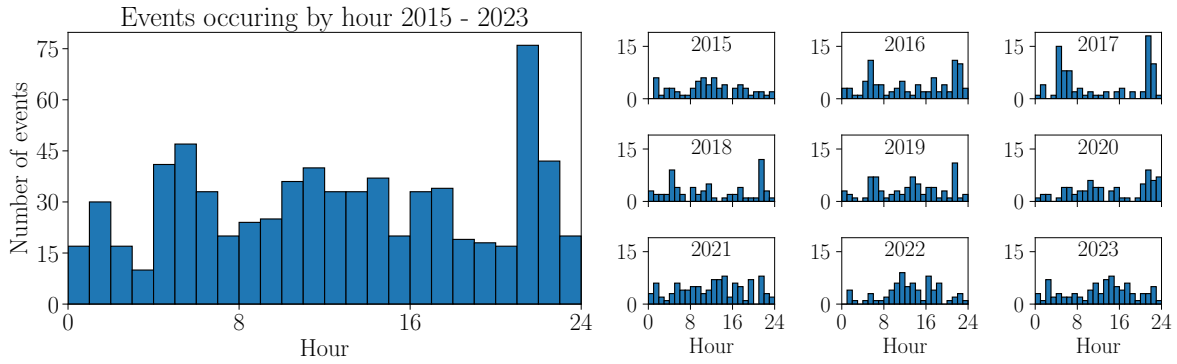

Figure 8: Hour intervals in which RoCoF events have occurred in the Nordic Synchronous Area from 2015–2023. The vertical axis represents the number of events, and the horizontal axis represents their occurrence in the day. The subplots to the right contain histograms of each individual year.

The cumulative histogram shows great variance in the number of events for the whole period. Notably, the cumulative histogram shows fewer events at hours 0, 3 and 4 in the morning. The cumulative histogram also shows a clear spike in the number of events at hour 21.

To achieve an even greater overview of when events are happening, events can be displayed in a heatmap. Events sorted by month of occurrence can show if there are specific times of the year in which the grid is more susceptible to RoCoF events. The heatmaps in Fig. 9 display the occurrence of RoCoF events, sorted by month and year. The events are separated on the maximum RoCoF value found in the event. Four heatmaps are created, with the RoCoF increments being 40-100 mHz s^{-1}, 100-160 mHz s^{-1}, 160-220 mHz s^{-1}, and 220-280 mHz s^{-1}.

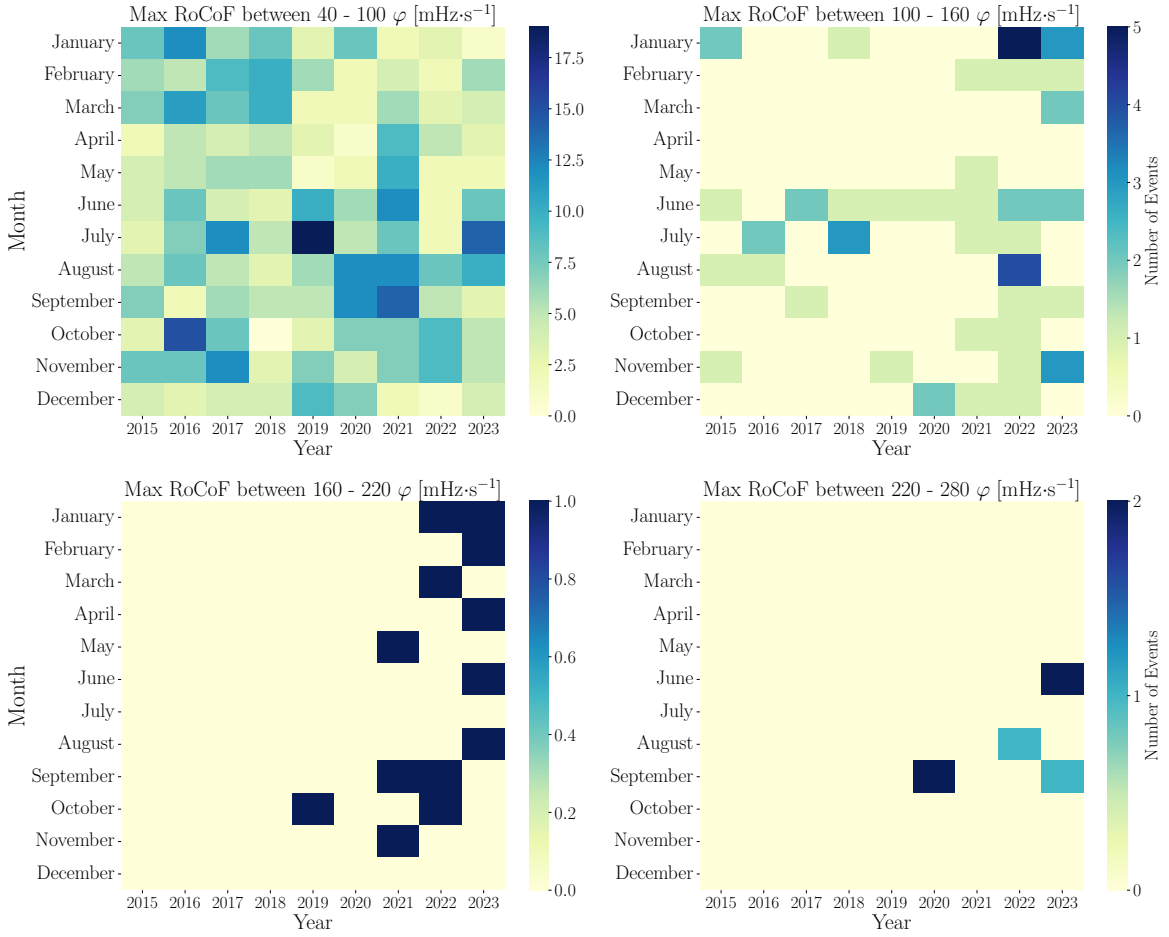

Figure 9: Heatmaps of RoCoF events found in the Nordic Synchronous Area from 2015 until 2023. Years are given on the vertical axis and months on the horizontal axis. The heatmaps have events sorted by maximum RoCoF, with the ranges displayed above each heatmap.

For the maximum RoCoF range of 40-100 mHz s^{-1}, it can be observed that April and May have fewer events occurring. When excluding the year 2021, this becomes even more prevalent. From the two highest RoCoF intervals, it can be observed that the total number of events is fewer. No events are detected in the years 2015-2018 for the highest intervals. The first occurrence of an event in the two highest intervals was in October 2019. The number of events in the higher intervals showcases a growing trend of events. In the range of 160-220 mHz s^{-1}, 1 event is found in 2019, 3 in 2021, 4 in 2022, and 5 in 2023. The range 220-280 mHz s^{-1} contains even fewer events, with 2 events found in 2020, 1 in 2022, and 3 in 2023.

5.2 RoCoFs correlation with nadir and time-to-nadir

Fig. 10 and 11 display the parameters maximum RoCoF vs. nadir and time-to-nadir in scatterplots. By doing this, the relationship between the variables can be explored. Initial negative events are marked red, while positive ones are marked blue. Notably, there is, in principle, no discernible difference between positive and negative events. The figures are complimented with fitted lines for positive and negative events.

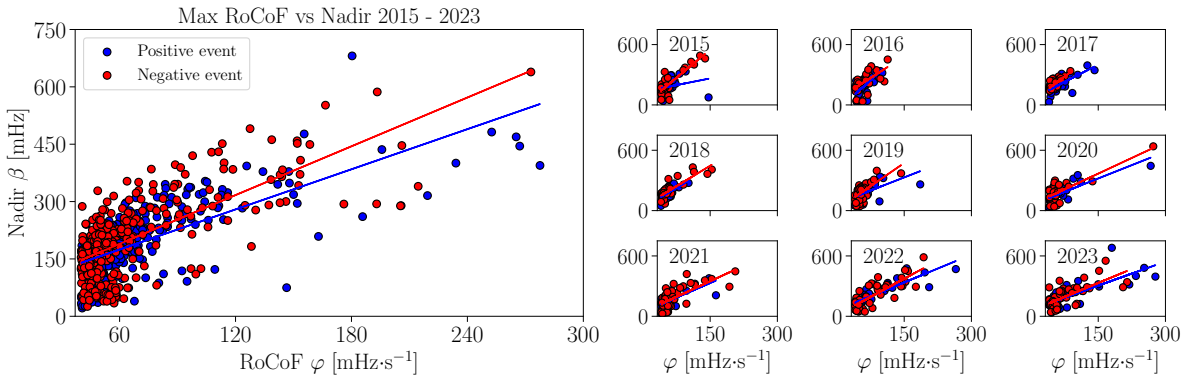

Figure 10: Maximum RoCoF vs. nadir found within events in the Nordic Synchronous Area from 2015–2023. The horizontal line represents RoCoF in $\mathrm{mHz\,s^{-1}}$, and the horizontal axis represents the nadir in mHz. Red and blue points indicate if an event was initially detected due to a negative or positive RoCoF value. The subplots contain events in each individual year.

Fig. 10 shows that the majority of events do not exceed a nadir value of 300mHz and a RoCoF value of $120\mathrm{mHz\,s^{-1}}$. The scatterplot shows the same trend as Fig. 7 with RoCoF severity increasing in later years, and the nadir is observed with a positive correlation to increasing RoCoF values.

Fig. 11 shows the parameters maximum RoCoF vs. time-to-nadir in a scatterplot. As previously, the scatterplot can show if there is a relationship between the variables, and initial negative and positive events are marked red and blue. There is, in principle, no difference between them. Worth noting is that the time-to-nadir is calculated by finding the minimum and maximum values of frequency inside the event. The grey area in the cumulative scatterplot marks ENTSO-Es expected time-to-nadir values [11].

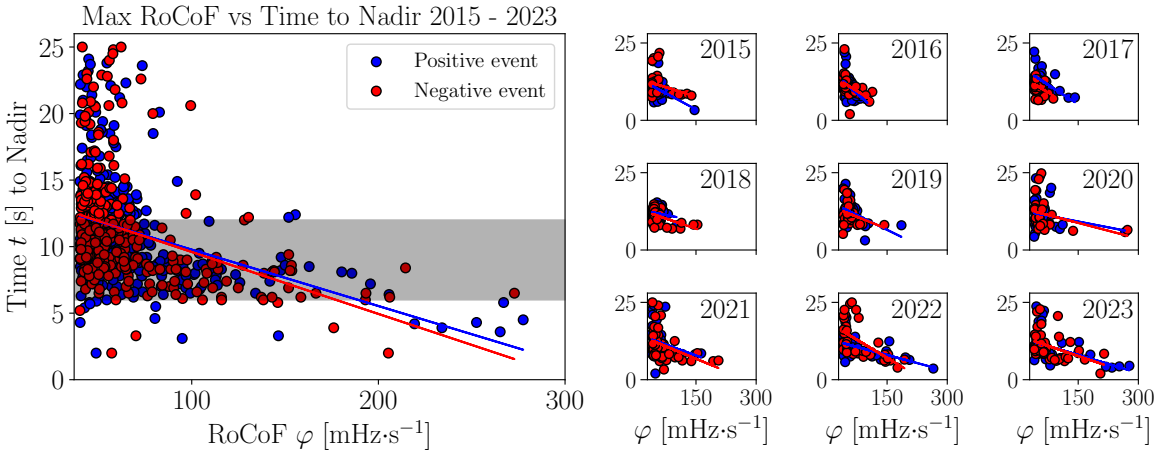

Figure 11: Maximum RoCoF vs. time-to-nadir found within events in the Nordic Synchronous Area from 2015–2023. The horizontal line represents RoCoF in mHz s^{-1}, and the horizontal axis represents the time-to-nadir in seconds. Red and blue points indicate if an event was initially detected due to a negative or positive RoCoF value. The grey area in the cumulative plot, 6–12 seconds, indicates the time-to-nadir values expected by ENTSO-E. The subplots contain events in each individual year.

The majority of events have a time-to-nadir in the time window of 6-12 seconds. For the more severe events above 200 mHz s^{-1}, no events have a time-to-nadir above 10 seconds. The few events that are above 250 mHz s^{-1} have a time-to-nadir around 5 seconds. It can also be observed from the subplots that the maximum RoCoF has increased in later years. The year 2018 stands out as the events this year are accumulated in terms of time-to-nadir.

5.3 Individual events

All the events which are found can be individually plotted to show how the frequency and RoCoF values change after an event occurs. This can offer insight for the trained eye to evaluate the behaviour of both the frequency and RoCoF. The individual events in Fig. 12 are chosen from events in 2015–2023. They are selected on the severity of both the maximum RoCoF and nadir values. The plots are displayed with dual y-axes, representing the frequency and RoCoF. The reference frame of the frequency is 50 Hz, and the event date is in the format DD-MM-YYYY.

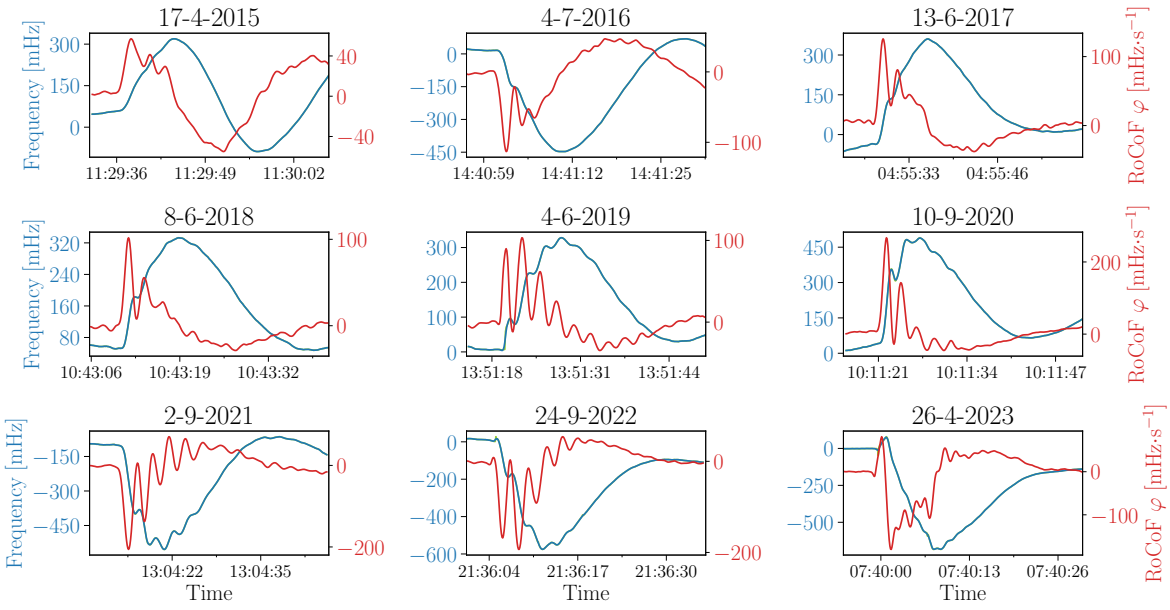

Figure 12: Individually plotted RoCoF events from the Nordic Synchronous Area. The dual vertical axes display the frequency and RoCoF values. The blue coloured lines and text represent frequency values, while those in red show the calculated RoCoF values. The events presented are some of the most critical regarding maximum RoCoF and nadir values. Timestamps are given in UTC+2 or UTC+3, depending on daylight saving time.

All individual events chosen have nadir values exceeding 300 mHz. More severe events can be seen in later years, with frequency values exceeding 450 mHz from 2020 to 2023. The maximum RoCoF values can also be observed to be larger in the years 2020-2023. Events in years prior to 2020 can be seen to have maximum RoCoF values of around 100 mHz s^{-1}.

6 Discussion

6.1 Interpretation of key findings

The analysis of RoCoF events across the NSA indicates that there are some yearly fluctuations, but the total number of RoCoF events remains relatively consistent, with no discernible upward trend. The lowest number of events in the 2015–2023 period occurred in 2015, totalling 66 events, while the peak occurred in 2021 with 102 events. Further categorization of events is also done according to their maximum RoCoF values. The division is done in the following ranges: 40–100 mHz s^{-1}, 100–160 mHz s^{-1}, 160–220 mHz s^{-1}, and 220–280 mHz s^{-1}. A closer examination of later years reveals a substantial increase in the number of events within the three highest RoCoF ranges when compared to previous years. Specifically, the range of 100–160 mHz s^{-1}, which averaged about 4 events annually from 2015 to 2021, saw a significant increase to 17 events in 2022 and 12 events in 2023. A similar trend is observed in the 160–220 mHz s^{-1} range. This range contains one event in 2019, with subsequent years showing a gradual increase: one event in 2019, none in 2020, 3 in 2021, 4 in 2022, and 5 in 2023. The highest RoCoF range, 220–280 mHz s^{-1}, also shows variability, with two events occurring in 2020, one in 2022, and three in 2023, totalling six events within this range.

As the categorization by RoCoF ranges sheds light on the intensity of events, event occurrence by hour complements the aforementioned results by detailing at what time of day the events occur. Thus providing a fuller picture of RoCoF dynamics over time. The aggregated hourly histogram from 2015–2023 highlights a pronounced peak in events during the 21:00 to 22:00 hour. A deeper analysis reveals that this trend is predominantly driven by the years 2016 to 2019, during which approximately 15 events were found in this specific hour. The years 2016 to 2019 also demonstrate a heightened occurrence of RoCoF events during the early morning and late evening hours, with there being fewer events during the daytime. In contrast, the data spanning from 2020 to 2023 indicates a more uniform distribution of events throughout the day, without a distinct peak in any specific hour. This is in line with the event distribution seen in 2015. This, put together, suggests a temporal shift in the pattern of RoCoF events for the years 2016–2019.

The hourly breakdown highlights specific times of day when RoCoF events are more prevalent. Another interesting trend is the seasonal effects on RoCoF events. Analysis of the seasonal occurrence of events reveals no pronounced peaks in any month. Power usage in the Nordic countries is generally higher in the winter months, which, in theory, should stress the grid more, which again could lead to more events occurring. Evidence of this occurring is not found, but interestingly some of the summer months appear with fewer events. The months of April and May overall have the lowest amount of events. If one excludes the year 2021, this trend becomes even more prevalent. This is in line with what is expected, as power consumption is generally lower in these months. From this alone, a conclusion on events occurring less often in the summer months cannot be drawn, as June, July, and August have numerous events occurring. Combined then, RoCoF events in the NSA do not seem to be closely connected to the seasons.

Continuing the analysis, the maximum RoCoF of events is compared against the parameters

'nadir' and 'time-to-nadir'. These parameters can reveal whether the severity of RoCoF events is correlated. It is expected that a larger RoCoF value in an event will lead to a higher nadir value. In the analysis, this is proven, as there is shown a positive correlation between maximum RoCoF and nadir. The trend of the aforementioned analysis, with later years having increased RoCoF values, is followed by the nadir. A closer examination shows that 2020–2023 has events with the highest nadir values. With 2023 showing an event reaching a nadir value over 600 mHz. This is somewhat worrying if the trend of increasing severe RoCoF events is sustained. As such RoCoF events of this severity could cause serious disruptions to the grid.

The parameter time-to-nadir in the analysis shows a negative correlation with increasing RoCoF values. Events with higher RoCoF values in the years 2020–2023, in particular, showcase this correlation. If one follows ENTSO-E's expectation, most events should have time-to-nadir values that fall within the range of 6–12 seconds. While most events fall within this area, there are several events that have higher or lower time-to-nadir values. Interestingly, more severe events, with RoCoF values over 200 $\mathrm{mHz\,s^{-1}}$, tend to fall under the expected time-to-nadir time of 6 seconds. This is still somewhat in line with expectations, as the grid operators are probably acting more aggressively when large events occur to avoid grid instability.

When examining some of the individual events, it can be observed that inertia and other countermeasures, like FFR, play a role in dampening the frequency changes. Comparing the frequency data before and after the time of the nadir shows that in most cases, there is unquestionably dampening occurring, assisting in the stabilisation of the grid frequency. The dampening can be viewed in the small stabilising periods prior to nadir. In the post-nadir of the event, stabilising periods are not present. This showcases that the dampening pre-nadir is a system response to an undesired frequency change. These small periods of dampening are also emphasised by an oscillating RoCoF value. This stabilizing effect is not only expected but also crucially needed to avoid grid instabilities or shutdowns. The largest event found in the analysis occurred on the 26. April in 2023. Where the frequency can be observed to drop down to 680 mHz below the nominal frequency of 50 Hz. If, as already mentioned, this trend is found to be sustained, events of this calibre could become more frequent and cause problems for the TSOs in NSA in the coming years.

With the penetration of RES expected to continue its rise, the relative percentage of inertia from total generation will lower. Speculating 50 years into the future. If the NSA ever reaches penetration levels of the scale of a hundred GW of non-inertia power sources, one could really start to see RoCoF incidents rising drastically. Combined with the infrastructural issues which are found and reported on by Fingrid, the grids of the NSA would be in real hardship. Fortunately, the TSOs are capable bodies, and being proactive, they could possibly employ sophisticated synthetic battery electronics to combat the lower inertia. Better still, with the present hydropower and nuclear generations, the installation of large flywheels could be done. These flywheels could be sped up and maintained for usage when inertia in the system is low. The future might bring more troubles for the grids in the NSA, but TSOs hopefully cope and come up with solutions which will help society toward carbon neutrality.

6.2 Comparison with other studies

The scientific article, "Renewables in the European power system and the impact on system rotational inertia", by Mehigan et al. [28], looked closer at inertia duration curves and how different scenarios of RES implementations will impact the occurrence of RoCoF events in 2030. As seen in Fig. 2 the Nordic are projected with two different scenarios affecting the inertia duration curve. Scenario one is pessimistic and has the lowest integration of RES, while scenario two has the most optimistic view, with the highest amount of RES incorporated in the grid. The inertia duration curve shows that the Nordic is not projected to have low enough inertia to be at risk of a 0.5 $\mathrm{Hz\,s^{-1}}$ or 1.0 $\mathrm{Hz\,s^{-1}}$ events. The results in this thesis concur with the fact that currently, there are no events close to the limit of 0.5 Hz/s. There is, however, an increasing trend of severe RoCoF events happening in the grid. The TSOs in the NSA are undoubtedly cognisant of the rising number of severe RoCoF events.

In their 2022 report [31], Fingrid addresses 16 severe RoCoF events with nadir values over 300 mHz directly with technical information. The severe events are found to be solely caused by nuclear power generation and power line failures. From this information, it seems like the NSA is not prone to RoCoF events due to lower inertia but rather suffers severe RoCoF events due to infrastructure faults. Although other TSOs in the NSA have acknowledged the need for measures to manage reduced grid inertia, no comparison to the one by Fingrid has been found. This lack of public disclosure might be due to the need for TSOs to retain sensitive information internally rather than publicly highlight potential vulnerabilities in their grids. Such weaknesses could possibly be exploited by a foreign party with malicious intent. With an active war ongoing in Europe and the world political scene being tense, it makes sense that critical information regarding infrastructure is being held secret. These assumptions are speculative, and there may be other undisclosed reasons behind the absence frequency reports.

6.3 Limitations

In the analysis of RoCoF events, specific thresholds for RoCoF values and the nadir are established to determine whether an event warrants being detected. Smaller frequency deviations are typical in power grids, therefore, establishing a lower boundary for RoCoF helps in identifying significant events. Currently, the RoCoF limit used in the analysis is set at 40 $\mathrm{mHz\,s^{-1}}$, which is 5 $\mathrm{mHz\,s^{-1}}$ above the standard recommended by ENTSO-E [11]. Upon reflection, aligning this limit with the ENTSO-E standard would have facilitated better comparisons with other studies. However, the limit is still satisfactory when considering that the analysis does show a shift of frequencies in higher RoCoF ranges. While smaller events still can be somewhat impact-full to the grid, the more severe events are the ones that pose the greatest risk to grid stability.

Additionally, a nadir limit of 35 mHz is used to exclude RoCoF events in which the frequency deviations are minimal. This threshold filters out minor disturbances, focusing the analysis on more significant fluctuations. Another concern involves data quality from the Fingrid dataset [9]. Approximately 1 percent of the data is missing for the years 2015–2023. While this figure is generally acceptable, the distribution of missing data varies across different years and months. The practice performed in the analysis of forward-filling missing data with previous recordings is

introducing artificial frequency fluctuations. Potentially leading to erroneous detection of RoCoF events if the aforementioned limits are met. Efforts have been made to identify and remove events that are impacted by forward-filled data, but small gaps in frequency measurements that are filled might still affect the accuracy of the analysis.

A key part of finding RoCoF events is to have consistent and noise-reduced frequency data. In signal processing, smoothers are utilized to mitigate unwanted noise caused by grid fluctuations and recording errors. They are mainly used to reduce the influence of outliers in the data, which, if left untouched, could lead to the misinterpretation of RoCoF events. Smoothers should not be used recklessly, as overdoing smoothing can lead to a diminishing of trends in the data. The WH employed in the analysis for this thesis is selected for its specific parameter advantages, where 'order' and 'lambda' are tunable. The smoother is also effective at smoothing data near the edges of data frames. This makes it capable of utilising parallel processing when data is divided into chunks. In use, the WH smoother operates as anticipated. With outliers in the data being promptly reduced, and trends of the frequency data being preserved. However, the smoother operation is only tuned by visual inspection, which leaves a small chance of the smoother not being optimally tuned. Which could lead to the parameters of RoCoF events being wrongly calculated. One could argue for the use of cross-validation to find the best parameters, but as the data stretches over nine years and is subject to measurement device change, this was deemed not feasible. If a cross-validation had been conducted, it might have required a new cross-validation run for each year, possibly even for each month.

The sheer size of the dataset presents inherent limitations on the depth of analysis possible in the time span of this thesis. Spanning from 2015 to 2023, the complete zipped dataset is 9.26 GB. When decompressed, assuming an approximate compression rate of 9 expands to about 83 GB. A considerable effort has been dedicated to refining the RoCoF analysis to identify events across all years correctly. During the exploration of the dataset, wrongly marked events and anomalies like the aforementioned forward-filling issue were uncovered and taken care of. Although all detected events during analysis have been reviewed to identify any irregularities, they have not been subjected to detailed analysis. Consequently, there is a risk of incorrectly detected events or, events not being detected at all.

6.4 Suggestions and future work

While the RoCoF analysis methods used in this thesis are satisfactory, there is potential for enhancements when capturing details. Currently, the method for identifying the nadir point is adequate but lacks comprehensiveness. The method is limited in identifying only the minimum or maximum points within the event. This is, in some cases, creating incorrect nadir and time-to-nadir values. One potential approach to solve this could be to identify local nadir points and measure their distance from the event's initial start point. Subsequently, a threshold could be established to determine how far the nadir is expected to be from the start point. This refinement could lead to more precise nadir marking, though it, as the current method, may also incorrectly mark nadir. Ideally, nadir values would be set and identified manually, which, while increasing accuracy, would negate the benefits of automating the analysis process.

A pre-analysis could have been performed to achieve an even higher level of confidence in the final analysis. This would have led to better results from the analysis, with a more in-depth analysis of each event and possibly removing or re-adding previously removed events.

In total, 204 events have been removed, because of their high or low 'time-to-nadir' values. The main concern regarding the excluded events lies in the events which had a time-to-nadir value that was considered too low. These are mainly removed on the basis that RoCoF events' time-to-nadir values are expected to be above a certain level. A considerable amount of time has not been spent exploring if events below the threshold of two seconds should still be considered valid. As Fig. A.5 highlights, several severe events are dismissed from 2023. The analysis performed is still valid, but if events below two seconds were to be included, the trend of increasing severe RoCoF events would be even more prevalent.

Inertia is not regarded when accessing the RoCoF events, as this thesis focuses solely on exploring and identifying RoCoF events. It could be interesting to perform a deeper study exploring inertia's impact on RoCoF events. Such an analysis could reveal if event behaviour and occurrence are changing with different inertia levels.

7 Conclusion

The total number of RoCoF events in the NSA is not found to be increasing in total number for the time period 2015 to 2023. However, the analysis reveals a remarkable shift of events toward higher RoCoF ranges. From 2015–2021, the 100–160 mHz s^{-1} range averaged about four events per year. This number is shown to have increased substantially to 17 events in 2022 and 12 in 2023. A similar trend is observed in the 160–220 mHz s^{-1} and 220–280 mHz s^{-1} ranges. Where for the range, 160–220 mHz s^{-1}, a gradual increase is seen from one event in 2019, 3 events in 2021, 4 events in 2022, and 5 events in 2023. The range, 220–280 mHz s^{-1} is found with 2 events in 2020, 1 event in 2022, and 3 events in 2023.

The escalation in severe RoCoF events is not surprisingly also linked to their nadir values. The years 2020 through 2023 display progressively higher values of nadir. The highest deviation in frequency is found on the 26. April in 2023, where a RoCoF event caused the frequency to drop by 682 mHz. The causes behind RoCoF events shifting towards higher ranges have not been further investigated in this thesis, but published reports by ENTSO-E and Fingrid shed some light on the findings. A report published in 2017 by ENTSO-E, did not identify any discernible reasons to believe that reduced grid inertia would lead to a substantial increase in RoCoF events for the years 2020 and 2025. This report then reduces the expectation of inertia alone being the factor behind the increase in severe RoCoF events.

A frequency quality report published by Fingrid in 2022 gives context to the severe events which occurred in their grid in 2022. They found the cause of all severe events to be associated with faults in nuclear generation or power lines. This suggests that the increasing amount of severe RoCoF events is mainly caused by faults in the infrastructure of the power grid and not by reduced inertia.

The methods and analyses presented in this thesis also demonstrate that a RoCoF analysis can be performed using a common modern computer. By adopting a live RoCoF estimation, grid operators can identify and respond to events in real time. As the analysis shows, events that have occurred have not caused a critical grid failure. The events have been properly taken care of, which shows that the TSOs within the NSA are actively monitoring and controlling their grids. Amidst commitments by the countries in the NSA to reduce greenhouse gas emissions, including the integration of more RES into their power systems, the analysis shows a rise in the severity of RoCoF events. This correlation highlights the need for ongoing investigation and analysis to ensure the stability and reliability of the grids in the NSA as they incorporate increasing amounts of RES in the years ahead.

In summary, the analysis shows that RoCoF events have been annually increasing in severity, with the trend being especially prevalent from 2020 to 2023. As a response, the TSOs within the NSA should continue monitoring their grids and perform further research on necessary measures to reduce severe RoCoF events.

References

[1] H. L. [Core Writing Team and J. R. (eds.)]. IPCC, 2023: Sections. In: Climate Change 2023: Synthesis Report. Contribution of Working Groups I, II and III to the Sixth Assessment Report of the Intergovernmental Panel on Climate Change. DOI: 10.59327/IPCC/AR6-9789291691647. 2023.

[2] The International Energy Agency. World Energy Outlook 2023. IEA, Paris, October 2023. URL: https://www.iea.org/reports/world-energy-outlook-2023 (visited on 04/19/2024).

[3] EirGrid and System Operator for Northern Ireland. Potential Solutions for Mitigating Technical Challenges Arising from High RES-E Penetration on the Island of Ireland. URL: https://cms.eirgrid.ie/sites/default/files/publications/Technical-Assessment-of-2030-Study-Outcomes.pdf (visited on 02/03/2024).

[4] European Commission and Directorate-General for Climate Action. Going climate-neutral by 2050 – A strategic long-term vision for a prosperous, modern, competitive and climate-neutral EU economy. DOI: 10.2834/02074. 2019.

[5] Ministry of Economic Affairs and Employment of Finland. Carbon neutral Finland 2035 – national climate and energy strategy. URL: https://urn.fi/URN:ISBN:978-952-327-843-1 (visited on 04/17/2024). 2022.

[6] Swedish Climate Policy Council. 2023 Annual report of the Swedish Climate Policy Council. URL: https://www.klimatpolitiskaradet.se/en/report-2023/ (visited on 04/17/2024). 2023.

[7] The 2050 Climate Change Committee. The transition to low emissions. Climate policy choices towards 2050, Norwegian Official Report (NOU) 2023: 25. URL: https://klimautvalget2050.no/forside-english/ (visited on 04/17/2024). 2023.

[8] Danish Council on Climate Change. Status Outlook 2022, Denmark's national climate targets and international obligations. URL: https://klimaraadet.dk/en/report/status-outlook-2022 (visited on 04/17/2024). 2022.

[9] FinGrid. FinGrid Historical Frequency data. URL: https://beta-data.fingrid.fi/en/datasets/339 (visited on 02/15/2024). 2024.

[10] Eylert Ellefsen. Expected production and power balances for the Nordpool areas until 2040. URL: https://www.energyquantified.com/blog/expected-production-and-power-balances-for-the-nordpool-areas-until-2040 (visited on 05/10/2024). 2023.

[11] ENTSO-E. Future nordic system inertia. URL: https://eepublicdownloads.entsoe.eu/clean-documents/Publications/SOC/Nordic/Nordic_report_Future_System_Inertia.pdf (visited on 02/20/2024). 2013.

[12] Norwegian Ministry of Energy. The power market and prices. URL: https://www.regjeringen.no/en/topics/energy/electricity/the-power-market-and-prices/id2076000/ (visited on 04/30/2024). 2016.

[13] North Sea Link. North Sea Link. URL: https://www.northsealink.com/en/north-sea-link/overview/ (visited on 04/30/2024). 2024.

[14] ENTSO-E. Nordel. URL: https://docstore.entsoe.eu/news-events/former-associations/nordel/Pages/default.aspx (visited on 04/29/2024). 2018.

[15] Directorate-General for Energy. 2 years since Ukraine and Moldova synchronised electricity grids with EU. URL: https://energy.ec.europa.eu/news/2-years-ukraine-and-moldova-synchronised-electricity-grids-eu-2024-03-15_en (visited on 04/25/2024).

[16] ENTSO-E. Regional Groups. URL: https://docstore.entsoe.eu/about-entso-e/system-operations/regional-groups/Pages/default.aspx (visited on 04/25/2024). 2024.

[17] J. D. Glover, T. J. Overbye, A. B. Birchfield, and M. S. Sarma. Power System Analysis & Design, Seventh Edition,SI. ISBN:978-0-357-67619-6. Cengage, 2017.

[18] T. Wildi. Electrical Machines, Drives, And Power Systems, Sixth Edition. ISBN:0-13-196918-8. Pearson Education, Inc., 2006.

[19] IEEE. IEEE/IEC International Standard - Measuring relays and protection equipment - Part 118-1: Synchrophasor for power systems - Measurements. DOI: 10.1109/IEEESTD.2018.8577045. 2024.

[20] J. Barrios-Gomez, F. Sanchez, G. Claudio, F. Gonzalez-Longatt, M. Acosta, and D. Topic. RoCoF Calculation Using Low-Cost Hardware in the Loop: Multi-area Nordic Power System. Osijek, Croatia. DOI: 10.1109/SST49455.2020.9264119. 2020.

[21] E. T. Whittaker. On a New Method of Graduation. *Proceedings of the Edinburgh Mathematical Society* (41), 63–75, 1922. DOI: 10.1017/S0013091500077853.

[22] M. Schmid, D. Rath, and U. Diebold. Why and How Savitzky–Golay Filters Should Be Replaced. *American Chemical Society Measurement Science Au* **2**(2), 185–196, 2022. DOI: 10.1021/acsmeasuresciau.1c00054.

[23] P. H. C. Eilers. A Perfect Smoother. *Analytical Chemistry* **75**(14), 3631–3636, 2003. DOI: 10.1021/ac034173t.

[24] Statnett. Introduksjon til reservemarkedene. URL: https://www.statnett.no/for-aktorer-i-kraftbransjen/systemansvaret/kraftmarkedet/reservemarkeder/introduksjon-til-reserver/ (visited on 02/06/2024).

[25] Statnett. Raske frekvensreserver-FFR. URL: https://www.statnett.no/for-aktorer-i-kraftbransjen/systemansvaret/kraftmarkedet/reservemarkeder/ffr/ (visited on 02/06/2024).

[26] W. Uijlings. An independent analysis on the ability of generators to ride through rate of change of frequency values up to 2Hz/s. URL: https://www.eirgrid.ie/site-files/library/EirGrid/DNV-KEMA_Report_RoCoF_20130208final_.pdf (visited on 01/22/2024).

[27] H. Yin, Y. Wu, W. Qiu, C. Zeng, S. You, J. Tan, A. Hoke, C. J. Kruse, B. W. Rockwell, K. A. Kawamura, and Y. Liu. Precise ROCOF estimation algorithm for low inertia power grids. *Electric Power Systems Research* **209**, 2022. DOI: 10.1016/j.epsr.2022.107968.

[28] L. Mehigan, D. Al Kez, S. Collins, A. Foley, B. Ó'Gallachóir, and P. Deane. Renewables in the European power system and the impact on system rotational inertia. *Energy* **203**, 117776, 2020. DOI: 10.1016/j.energy.2020.117776.

[29] ENTSO-E. TYNDP 2016 Scenario Development Report. URL: https://eepublicdownloads.entsoe.eu/clean-documents/tyndp-documents/TYNDP%202016/rgips/TYNDP2016%20Scenario%20Development%20Report%20-%20Final.pdf (visited on 01/22/2024).

[30] Energinet, Fingrid, Statnett, and Svenska kraftnät. Nordic Grid Development Perspective 2023. URL: https://www.fingrid.fi/contentassets/6457e50d0dee45a38d69f709d9cd4c87/svk_ngpd2023_a4_korr4.pdf (visited on 04/18/2024). 2023.

[31] FinGrid. Frequency quality analysis - 2022. URL: https://www.fingrid.fi/globalassets/dokumentit/fi/kantaverkko/suomen-sahkojarjestelma/frequency_quality_analysis_2022_public.pdf (visited on 04/14/2024). 2022.

[32] C. R. Harris et al. Array programming with NumPy. *Nature* **585**, 357–362, 2020. DOI: 10.1038/s41586-020-2649-2.

[33] L. S. Michael M. McKerns, A. F. Tim Sullivan, and M. A. G. Aivazis. Building a framework for predictive science. *Proceedings of the 10th Python in Science Conference*, 2011. URL: http://arxiv.org/pdf/1202.1056 (visited on 05/09/2024).

[34] M. McKerns and M. Aivazis. pathos: a framework for heterogeneous computing, 2010. URL: https://uqfoundation.github.io/project/pathos (visited on 05/09/2024).

[35] J. D. Hunter. Matplotlib: A 2D Graphics Environment. *Computing in Science Engineering* **9**(3), 90–95, 2007. DOI: 10.1109/MCSE.2007.55.

[36] M. L. Waskom. seaborn: statistical data visualization. *Journal of Open Source Software* **6**(60), 3021, 2021. DOI: 10.21105/joss.03021.

[37] K. A. Bø. Exploring Rate of Change of Frequency RoCoF events in the Nordic Synchronous Area. URL: https://github.com/xxFrozt/Exploring-Rate-of-Change-of-Frequency-RoCoF-events-in-the-Nordic-Syncrenous-Area/tree/main#Exploring-Rate-of-Change-of-Frequency-RoCoF-events-in-the-Nordic-Syncrenous-Area.

[38] IEEE. IEEE/IEC International Standard - Measuring relays and protection equipment - Part 118-1: Synchrophasor for power systems - Measurements. URL: https://standards.ieee.org/ieee/C37.118.1/4902/ (visited on 04/08/2024).

[39] IEEE. IEEE Standard for Synchrophasor Measurements for Power Systems – Amendment 1: Modification of Selected Performance Requirements. URL: https://standards.ieee.org/ieee/C37.118.1a/5621/ (visited on 04/08/2024).

[40] IEEE. IEEE Standard for Synchrophasors for Power Systems. URL: https://standards.ieee.org/ieee/C37.118/3058/ (visited on 04/08/2024).

[41] Private correspondance. 2024.

[42] P. H. C. Eilers. A Perfect Smoother. DOI: 10.1021/ac034173t. 2003.

[43] Python.org. Python Global Interpreter Lock. URL: https://wiki.python.org/moin/GlobalInterpreterLock (visited on 04/11/2024).

[44] Saturn Cloud. MATLAB Matrix Multiplication Performance: 5x Faster Than NumPy. URL: https://saturncloud.io/blog/matlab-matrix-multiplication-performance-5x-faster-than-numpy/ (visited on 05/10/2024).

[45] Grammarly Inc. Grammarly. URL: https://www.grammarly.com (visited on 05/09/2024).

[46] OpenAI. ChatGPT. URL: https://www.openai.com/chatgpt (visited on 05/09/2024).

[47] GitHub Inc. GitHub Copilot. URL: https://copilot.github.com (visited on 05/09/2024).

A Appendix

A.1 Complimentary table

Table A.1: Number of events in different RoCoF ranges from 2015–2023. This is equivalently represented in the histogram in Fig. 7.

	RoCoF Range ($\mathrm{mHz\,s^{-1}}$)			
Year	40-100	100-160	160-220	220-280
2015	61	5	0	0
2016	89	3	0	0
2017	84	3	0	0
2018	62	5	0	0
2019	74	2	1	0
2020	68	3	0	2
2021	93	6	3	0
2022	51	17	4	1
2023	65	12	5	3

A.2 Results with no data exlusion

Fig. A.1–A.5 contain results with previously excluded data. The exclusion was due to high or low 'time-to-nadir' values. The cutout was made for values over 25 seconds and below 2 seconds.

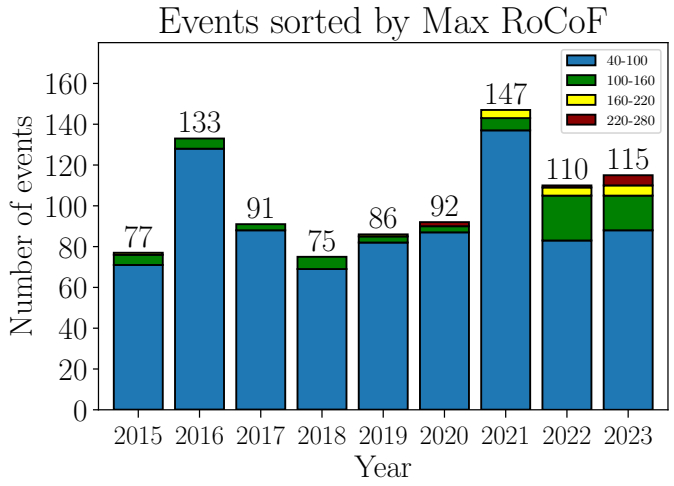

Figure A.1: Number of RoCoF events of each year from 2015–2023 in the Nordic Synchronous Area. The number above each bar is the total number of events for the years displayed along the horizontal axis. The events are further sorted by colour, with the maximum RoCoF values detected within each event falling within a RoCoF range, which is given in $\mathrm{mHz\,s^{-1}}$. The increments are displayed in the legend. Note: This figure contains results which were previously left out from the analysis.

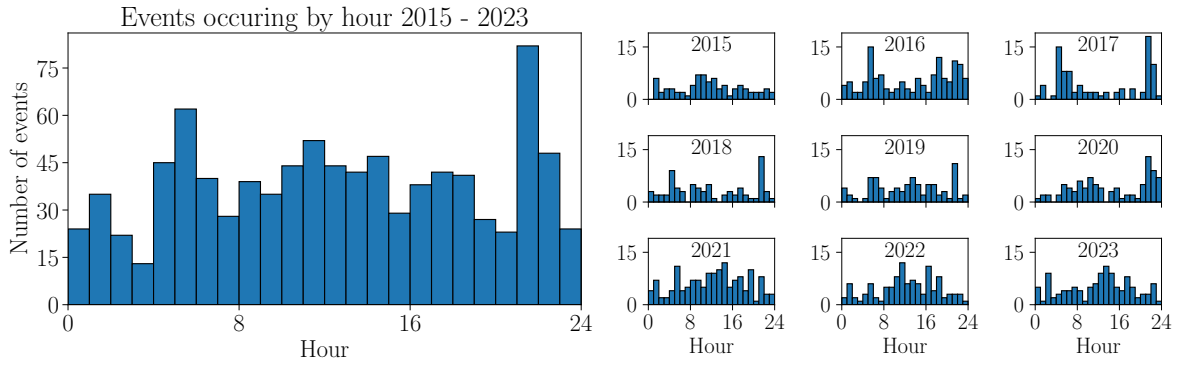

Figure A.2: Hour intervals in which RoCoF events have occurred in the Nordic Synchronous Area from 2015–2023. The vertical axis represents the number of events, and the horizontal axis represents their occurrence in the day. The subplots contain histograms of each individual year. Note: This figure contains results which were previously left out from the analysis.

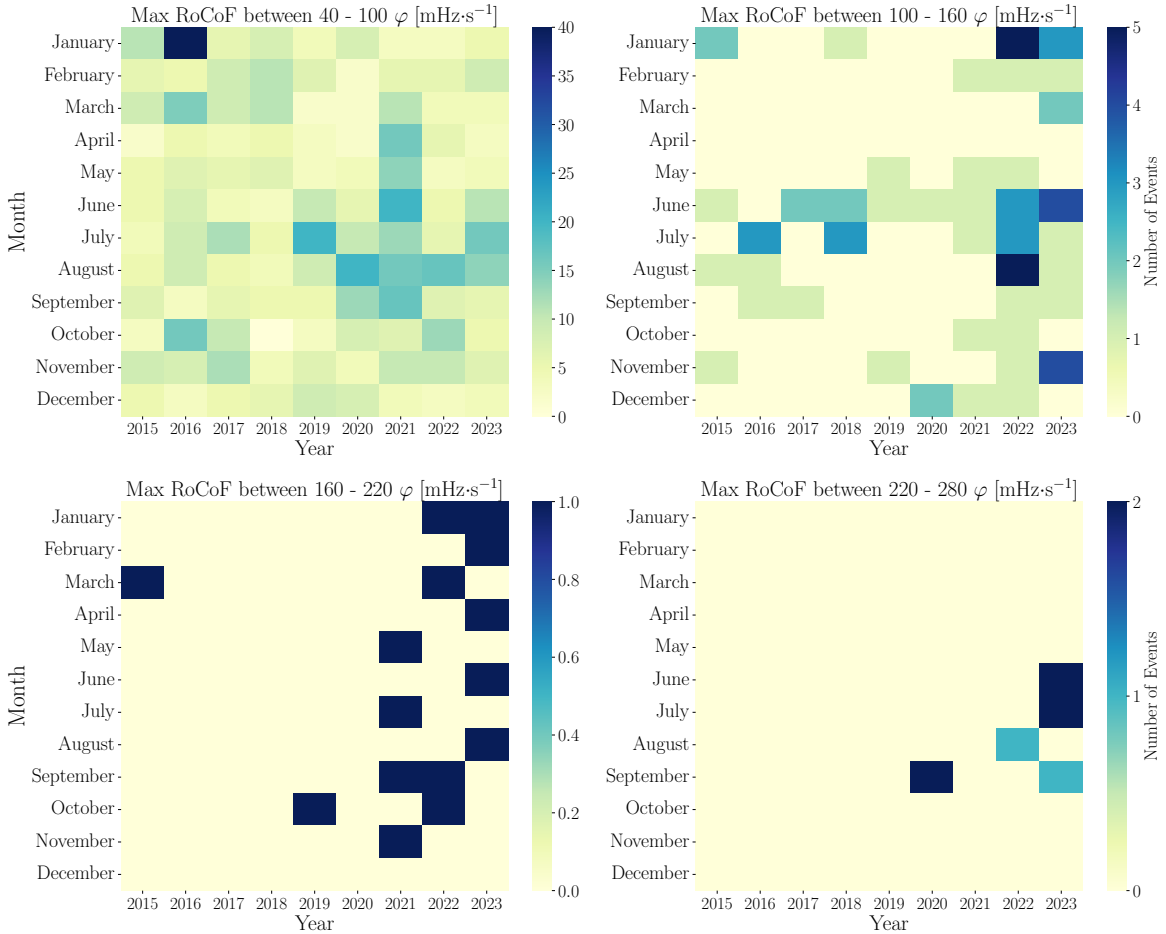

Figure A.3: Heatmaps of RoCoF events found in the Nordic Synchronous Area from 2015 until 2023. Years are given on the vertical axis and months on the horizontal axis. The heatmaps have events sorted by maximum RoCoF, with the ranges displayed above each heatmap. Note: This figure contains results which were previously left out from the analysis.

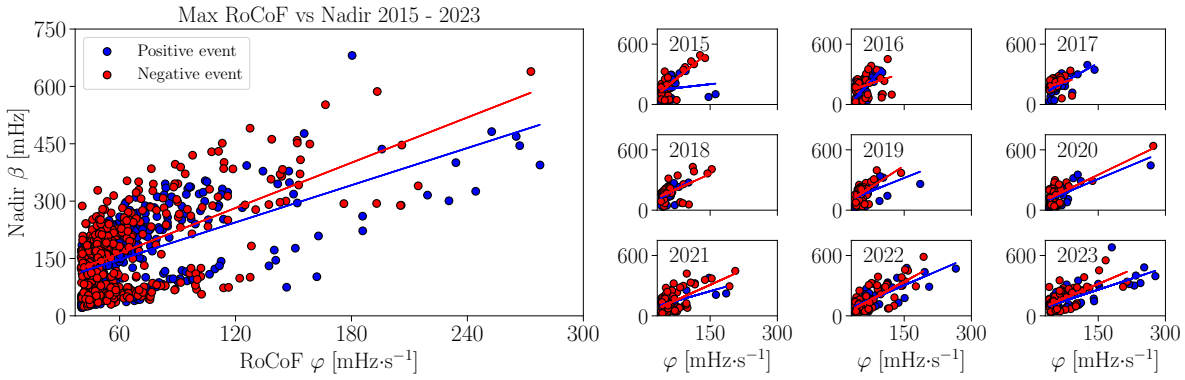

Figure A.4: Maximum RoCoF vs. nadir found within events in the Nordic Synchronous Area from 2015–2023. The horizontal line represents RoCoF in mHz s^{-1}, and the horizontal axis represents the nadir in mHz. Red and blue points indicate if an event was initially detected due to a negative or positive RoCoF value. The subplots contain events in each individual year. Note: This figure contains results which were previously left out from the analysis.

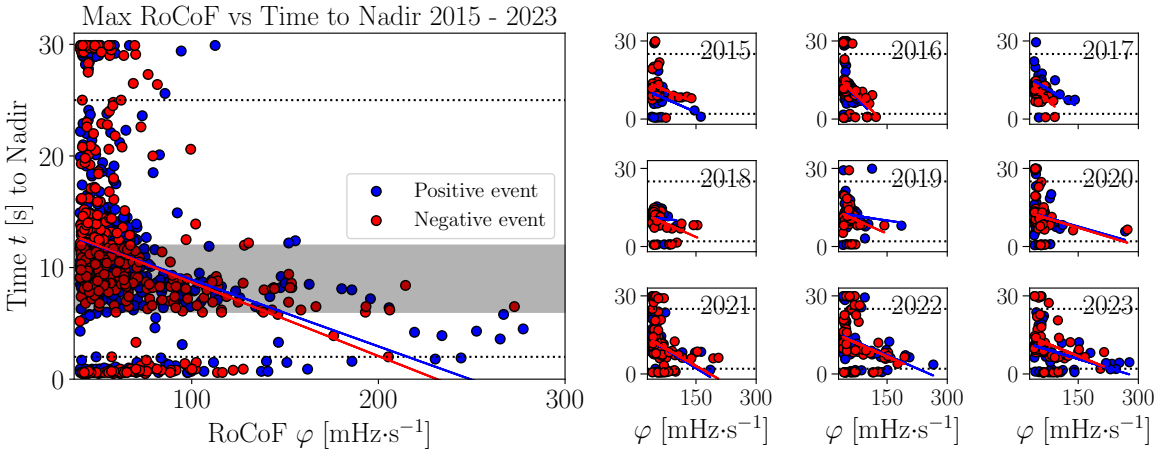

Figure A.5: Maximum RoCoF vs. time-to-nadir found within events in the Nordic Synchronous Area from 2015–2023. The horizontal line represents RoCoF in mHz s^{-1}, and the horizontal axis represents the time-to-nadir in seconds. Red and blue points indicate if an event was initially detected due to a negative or positive RoCoF value. The grey area in the cumulative plot indicates the time-to-nadir values expected by ENTSO-E, and the stipulated lines indicate where the cutoff was made to reduce the number of events for analysis. The subplots contain events in each individual year. Note: This figure contains results which were previously left out from the analysis.

Norges miljø- og biovitenskapelige universitet
Noregs miljø- og biovitskaplege universitet
Norwegian University of Life Sciences

Postboks 5003
NO-1432 Ås
Norway